SLAC–PUB–17366
December 2018

DYNAMIC APERTURE STUDIES FOR HL-LHC V1.0 *

Y. Cai†, R. De Maria‡, M. Giovannozzi‡, Y. Nosochkov†, F.F. Van der Veken‡;1
‡ CERN, CH-1211 Geneva 23, Switzerland
† SLAC National Accelerator Laboratory, Menlo Park, CA 94025, USA
1 Currently, also University of Malta, Msida, Malta

Abstract

Intense efforts have been devoted to the detailed study of the dynamic aperture of the HL-LHC V1.0 optics and layout version, without beam-beam effects, for several configurations, differing by optical properties or properties of the field quality of the new magnets for HL-LHC. In this report, the outcome of these studies is summarised and discussed.

* This research has been supported by the HL-LHC project. Part of this research is supported by the U.S. Department of Energy via the US-LARP program and the DOE Contract DE-AC02-76SF00515.

CERN-ACC-2018-0054

December 7, 2018

Dynamic aperture studies for HL-LHC V1.0

Y. Cai [†], *R. De Maria* [‡], *M. Giovannozzi* [‡], *Y. Nosochkov* [†], *F.F. Van der Veken* [‡,1]
[‡] CERN, CH-1211 Geneva 23, Switzerland
[†] SLAC National Accelerator Laboratory, Menlo Park, CA, USA
[1] Currently, also University of Malta, Msida, Malta

Abstract
Intense efforts have been devoted to the detailed study of the dynamic aperture of the HL-LHC V1.0 optics and layout version, without beam-beam effects, for several configurations, differing by optical properties or properties of the field quality of the new magnets for HL-LHC. In this report, the outcome of these studies is summarised and discussed.

Keywords
HL–LHC, dynamic aperture, field quality

CERN-ACC-2018-0054
07/12/2018

Contents

1 Introduction

This report presents dynamic aperture (DA) studies performed for the HL-LHC V1.0 lattice layout, which is closer to SLHCV3.1b, but with a new triplet layout based on 140 T/m Nb3Sn triplets [1]. Round and flat collision optics, injection optics, and pre-squeeze optics have been considered. The DA is obtained with tracking simulations using SixTrack [2, 3] and the related environment for massive numerical simulations, for both Beam 1 (the clockwise beam) and Beam 2 (the counter-clockwise beam). The following tracking conditions have been used, namely 10^5 turns, 5, 11 or 59 $x - y$ phase-space angles have been used, 30 particle pairs per $2\,\sigma$ amplitude step, 60 random error seeds for the generation of magnetic field errors, $2.5\,\mu$m-rad normalized emittance, $+3$ units of chromaticity, initial $\Delta p/p = 2.7\times 10^{-4}$ and 7.5×10^{-4} at 7 TeV (collision) and 450 GeV (injection) beam energies, respectively. For convenience, we list the nominal operational settings for the HL-LHC V1.0 optics version in Table 1. Unless otherwise specified, these are the settings used in all studies performed. Note that even though $\varepsilon_{\rm n} = 2.0\,\mu$m at injection, all results are expressed using $\varepsilon_{\rm n} = 2.5\,\mu$m for easy comparison.

The numerical simulations include non-linear field errors in arc magnets based on measured field quality (FQ) of the LHC magnets, and the estimated non-linear FQ of the new magnets in the interaction regions (IR) 1 and 5 where the high-luminosity experiments ATLAS and CMS are located. These are the inner triplet (IT) quadrupoles, the D1 and D2 separation dipoles, and the Q4 and Q5 matching quadrupoles.

The correction systems used in the simulations include the linear correction of tune, chromaticity, linear coupling and orbit; the non-linear field correctors b_3, b_4 and b_5 in the arc main dipoles; the non-linear field correctors up to the sixth order in the IR1/5 ITs [4].

Also, we define the minimum DA as the smallest DA among all seeds and phase-space angles, whereas the average DA is obtained by first averaging the DA over the seeds separately at each angle and then taking the minimum averaged value among the angles. Beam-beam effects are not included in any of the studies discussed in this report.

Table 1: Selection of parameters for HL-LHC V1.0 optics at injection and collision relevant for the simulations discussed in this report. The optics considered for collision conditions is the nominal round configuration.

Parameters	Injection	Collision
Beam total energy [GeV]	450	7000
Particles per bunch, N [10^{11}]	2.3	2.2
Bunches per beam	2748	2748
Colliding pairs in IP1/2/5/8	–	2736/2452/2736/2524
$\varepsilon_{\rm n}$ [μm]	2.0	2.5
$\varepsilon_{\rm L}$ [eVs]	0.7	2.5
σ_L (Gaussian r.m.s.) [cm]	10.4	8.1
Total RF voltage [MV]	8	16
Tunes (H/V)	62.28/60.31	62.31/60.32
β^* [m] in IP1/2/5/8	6/10/6/10	0.15/10/0.15/3
$\theta_{\rm c}/2$ at IP1/2/5/8 [μrad]	295/170/295/-250	295/170/295/-250
Half parallel separation at IP1/2/5/8 [mm]	2/2/2/-2	2/2/2/-2
Q'	3	3
$I_{\rm oct}$ [A]	-20	-570

It is worth stressing that the optics version considered for the studies presented in this report is older than that in the PDR [5], which is 1.1, and TDR [6], which is the V1.3.

It should be noted that the impact of the non-linear field quality of the 11 T dipoles on the DA has been studied and discussed in a separate paper [7] (the impact has been found marginal), whereas in the studies discussed in this report these effects have not been included.

The plan of this report is the following: in Section 2 the description of the field quality used in the LHC and HL-LHC DA simulations is recalled. In Sections 3-6 the studies are carried out considering only Beam 1 and 11 angles in the $x - y$ plane, whereas in Sections 7-9 both Beam 1 and Beam 2 are considered and 5 angles in the $x - y$ plane have been used, except for the studies reported in Section 7.1, where 59 angles have been used. Finally, some conclusions are drawn in Section 10.

2 Field quality description

In the framework of the LHC project, the magnetic field is defined by a multipole expansion [8]

$$B_y(x,y) + iB_x(x,y) = \sum_{n=1}^{N} (B_n + iA_n) \left(\frac{x+iy}{R_{\text{ref}}} \right)^{n-1} \tag{1}$$

$$= 10^{-4} B_{\text{ref}} \sum_{n=1}^{N} (b_n + ia_n) \left(\frac{x+iy}{R_{\text{ref}}} \right)^{n-1} , \tag{2}$$

where the A_n, B_n (absolute) and a_n, b_n (relative to the the main field at B_{ref}) multipole components are given at a reference radius R_{ref}. Furthermore, each of the a_n and b_n is a sum of three components, namely systematic (S), uncertainty (U), and random (R), such that the multipole value is given by

$$b_n = b_{n,\text{S}} + \frac{\xi_{\text{U}}}{1.5} b_{n,\text{U}} + \xi_{\text{R}} b_{n,\text{R}} , \tag{3}$$

where ξ_{U} and ξ_{R} are Gaussian-distributed random variables cut at $1.5\,\sigma$ and $3\,\sigma$, respectively, and $\sigma_{\xi_{\text{U}}} = \sigma_{\xi_{\text{R}}} = 1$. The ξ_{U} variable is the same for all magnets of a given class, but randomly changes from seed to seed and for the different multipoles. On the other hand, ξ_{R} changes also from magnet to magnet of the same class.

The measured multipole components, stored in the field-quality tables, assume a reference frame for which the x-direction points to the right when the magnet is seen from the connection end side. The beam dynamics codes like MAD-X use the opposite convention, therefore the following components need to change sign:

$$B_{2i}, A_{2i+1} \qquad \text{for any magnet} \tag{4}$$

$$b_{2i}, a_{2i+1} \qquad \text{for dipoles} \tag{5}$$

$$b_{2i+1}, a_{2i} \qquad \text{for quadrupoles} \tag{6}$$

where $i = 1, \ldots, N/2$.

For two-in-one magnets the field quality is given for the aperture named V1, which is on the left side when the magnet is seen form the connection side. The field quality description for the other aperture V2 is given assuming a mirror symmetry, therefore the following sign rules are applied for the S and U components of the field quality description:

$$b_{2i,\text{V2}} = -b_{2i,\text{V1}} \qquad a_{2i+1,\text{V2}} = -a_{2i+1,\text{V1}} \qquad \text{for dipoles} \tag{7}$$

$$b_{2i+1,\text{V2}} = -b_{2i+1,\text{V1}} \qquad a_{2i,\text{V2}} = -a_{2i,\text{V1}} \qquad \text{for quadrupoles} . \tag{8}$$

The a_n, b_n coefficients represent the magnet field quality at a given beam energy and up to $N = 15$. The FQ tables of the HL-LHC V1.0 optics can be found at the official HL-LHC repository [9].

Due to the very high beta functions in the IT quadrupoles in collision optics, the IT non-linear field errors create strong effects on the beam, which limit the dynamic aperture. The IT FQ has evolved

over time, as significant efforts are made by magnet designers to minimize the expected field errors, especially at collision energy. Based on these estimates, further optimization of the multipole coefficients was performed using DA tracking simulations in the effort of reaching a value of the DA around 12 σ, thus resulting in an optimized FQ specification [10]. The optimisation process was pursued starting from a more recent expected error table, giving a new optimised table providing a minimum DA of the order or $10.5\ \sigma$ [11]. For the sake of reference the error tables [11] are reported in Appendix A.

This report presents the studies performed over an extended period of time. For this reason, two versions of the IT FQ are used, where the multipole coefficients are given at $R_{ref} = 50$ mm. The first (earlier) version, named `IT_errortable_v66_5`, is presented in Table B.2 for 7 TeV and 450 GeV beam energies. It is based on the earlier FQ estimate `IT_errortable_v4` [9] which was then optimized using DA tracking simulations, resulting in reduced (by 20% to 50%) 7 TeV terms $b_{10\mathrm{S}}$, $b_{14\mathrm{S}}$, $b_{6\mathrm{U}}$ - $b_{14\mathrm{U}}$, $b_{6\mathrm{R}}$ - $b_{14\mathrm{R}}$, $a_{7\mathrm{U}}$ - $a_{9\mathrm{U}}$, and $a_{7\mathrm{R}}$ - $a_{11\mathrm{R}}$, based on a target DA value. In this version of the FQ, the multipole coefficients represent the total quadrupole field including the main body and the end field.

The latest estimate of the IT FQ `IT_errortable_v5` is presented in Tables B.3 and B.4 at collision and injection energies, respectively. This version improves the accuracy of the FQ representation by providing the separate field description for the main quadrupole body and the two ends. These components differ depending on whether the connection or non-connection sides are considered. The body FQ is the same as that of the earlier `IT_errortable_v4` estimate except that the systematic terms are updated (see Table 2). The end fields are represented by the three allowed systematic terms of order $n = 6, 10, 14$.

Table 2: Comparison of IT FQ expected table at injection and collision energies for the systematic component.

	`IT_errortable_v4`		`IT_errortable_v5`	
	7 TeV	450 GeV	7 TeV	450 GeV
$b6$	0.400	-15.800	-0.640	-21.300
$b10$	-0.390	3.630	-0.110	3.890
$b14$	-0.670	-0.600	-0.870	0.210

The IT FQ includes non-zero $b_{2\mathrm{R}}$ and $a_{2\mathrm{R}}$ terms affecting linear focusing and coupling. In machine operation, these effects will be compensated using appropriate correction systems. Hence, in the DA tracking simulations these terms are set to zero assuming full correction of these effects. This is the standard strategy used since the DA studies for the LHC (parenthetically, we stress that the all linear multipole components are neglected for all magnet classes). In future, there will be simulation campaigns dedicated to the analysis of the impact of linear coupling on DA and the a_2 multipole could be added to the simulations to make them even more realistic. Concerning the effect of b_2, before including this multipole in the DA simulations a tool to perform the correction of the beta-beating induced by b_2 should be made available.

For the studies presented in Sections 3-6 the FQ tables for the new D1, D2, Q4 and Q5 magnets, used in the simulations, are as follows:

- `D1_errortable_v1_spec`
- `D2_errortable_v5_spec`
- `Q4_errortable_v2_spec`
- `Q5_errortable_v0_spec`,

respectively [9]. Similarly, the non-zero b_2 and a_2 terms in these magnets, affecting linear optics, are set to zero in the tracking simulations assuming full correction. On the other hand, the studies presented in

Sections 7-9 do not use the specification error tables, but rather the expected ones. It should be noted though that this difference is minimal, as the only difference is in D1, and only in the systematic b_7 and b_9 errors at collision, which are reduced by a factor of two in the `D1_errortable_v1_spec` tables. It is worth stressing that, on the other hand, the expected and specified error tables for the triplet quadrupoles are very much different.

3 Optimization of phase advance between IP1 and IP5

The effects of non-linear field errors in the IT quadrupoles are significantly amplified by the very large beta-function values in collision optics, thus limiting the HL-LHC dynamic aperture. It has been also noted that the HL-LHC DA at injection energy was about $1\,\sigma$ smaller than the injection DA of the LHC. The latter may be due to modifications in the HL-LHC IRs. One way to improve the collision DA is to reduce the IT field errors. However, these quantities are already close to the lowest limit achievable in the magnet design. Also, smaller IT errors at injection energy would not make much impact on the DA since their effects are not the dominant ones in the injection optics, where the IT beta functions are relatively small.

It has been noted [12] that it may be possible to improve both the collision and injection DA by optimizing the phase advance between IP1 and IP5. In the collision optics, the IT quadrupoles and the separation dipoles at IR1 and 5 are the strongest sources of non-linear field error effects. Due to the very high beta functions, the IT and D1 magnets are essentially at the same phase. Moreover, the phase advance between magnets on the upstream and downstream sides of the interaction point (IP) 1 and 5 is nearly 180°. With these considerations, the IR1 and 5 magnets form effectively the two largest, almost point-like, sources of field errors separated by the IP1-IP5 phase advance. These multipoles create phase-dependent non-linear optical perturbations, e.g. non-linear resonances. It is therefore possible that a perturbation of a given order created at IR1 is compensated by a perturbation of the same type at IR5, provided a proper choice of phase advance is made. The complication is that the optimal phase advance depends on the order of the field error and the random errors in IR1 and IR5 are different. Therefore, only a partial compensation of the complete set of IT non-linear field errors is expected to be achievable with such an optimization process. The optimal phase advance for a maximum DA is also dependent on the contributions from field errors in other regions of the machine. Last, but not least, it is worth mentioning that there phase constraints from machine protection considerations, e.g. for the phase between the bump kickers and the tertiary collimators. This type of considerations, however, were not taken into account until very recently and hence, will not be part of the discussion presented here.

Although at injection energy the IT errors are not dominant, nonetheless, the DA may still be improved. In this case, the IP1-IP5 phase optimization may lead to a better compensation of the field error perturbations created in one half of the ring by the perturbations in the other half.

Due to the random nature of the errors and the highly complicated non-linear effects on the DA, such optimization cannot be carried out analytically. Hence, we perform tracking simulations using SixTrack with the goal to maximize the DA at both collision and injection energies as the phase advance can be changed depending on the optics configuration and the energy. It is worth mentioning that the IP1-IP5 phase advance can be set independently for Beam 1 and Beam 2. At collision energy, two lattice options are studied, namely round and flat optics, where $\beta^*_{x,y} = 15$ cm and $\beta^*_{x/y} = 7.5/30$ cm, respectively. The IT FQ in Table B.2 is used in this study and the Landau octupoles are turned off, as this allows enhancing the sensitivity of the DA simulations to the field errors of the HL-LHC magnets. A matching routine for the IP1-IP5 phase advance is included in the simulations, and a 2D scan of the horizontal and vertical IP1-IP5 phase advance is performed. The phase advance is measured from IP1 to IP5 in the clockwise direction. A large number of simulations and CPU time is required for this study in order to cover a sufficiently wide range of x and y phase advance with a small step.

The DA scan for the round collision optics is presented in Fig. 1, where the minimum (left) and

average (right) DA are shown. The arrow in each plot points from the nominal to the maximum DA in the scan. Since the minimum DA is determined by one worst seed, which could be an outlier in the seed distribution of a given $x - y$ angle, and such a seed can be different for the different phase advances, the minimum DA exhibits more fluctuations with the phase advance as compared to the average DA. The nominal IP1-IP5 phase advance in 2π units is $\mu_{x/y} = 31.21\,/\,30.373$, where the nominal $DA_{\rm min/ave} = 10.30\,\sigma\,/\,13.18\,\sigma$. The maximum $DA_{\rm min} = 12.33\,\sigma$ is achieved at $\mu_{x/y} = 31.28\,/\,30.02$, which is $2\,\sigma$ bigger than the nominal DA. The average DA at this phase advance is $14.18\,\sigma$. Interestingly, the maximum $DA_{\rm ave} = 14.56\,\sigma$ is achieved at a different phase advance, namely $\mu_{x/y} = 31.15\,/\,29.90$. In this second optimal phase setting, the $DA_{\rm min} = 11.75\,\sigma$ is smaller than in the previous setting. Detailed analysis of the DA in the second case shows that the smaller $DA_{\rm min}$ is caused by a single *bad* seed. Figure 2 compares the nominal and optimized DA for the first optimal setting, where $DA_{\rm min}$ is maximized.

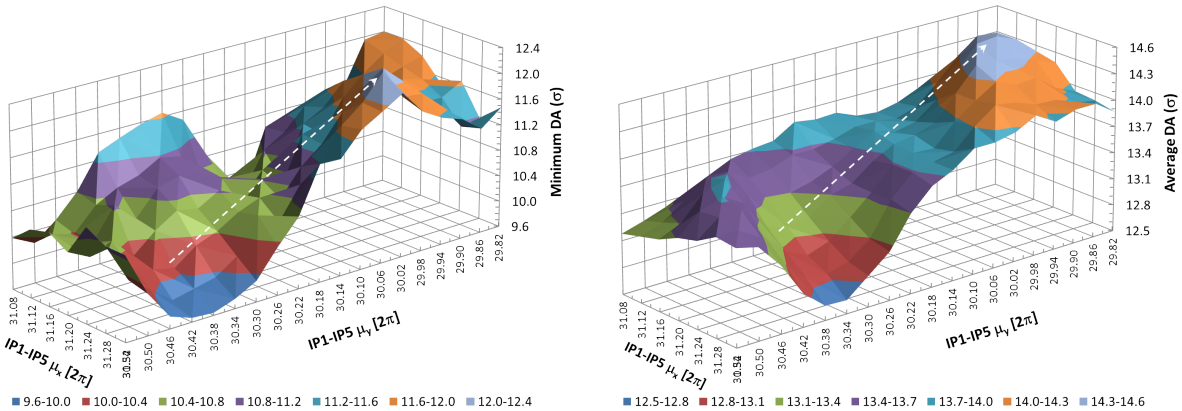

Fig. 1: Minimum (left) and average (right) DA of round collision optics vs IP1-IP5 phase advance. The arrow connects the nominal and maximum DA.

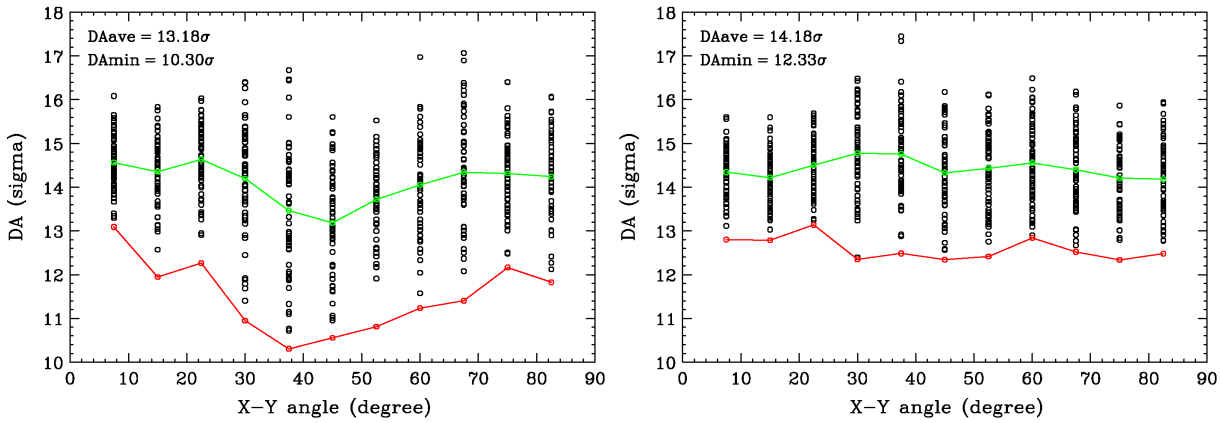

Fig. 2: DA of round collision optics for the nominal (left) and optimized, using $DA_{\rm min}$, (right) IP1-IP5 phase advance, where the circles represent the different seeds, and the green and red lines show the average and minimum DA at the 11 $x - y$ angles, respectively.

The DA scan for the flat collision optics is presented in Fig. 3. The nominal IP1-IP5 phase advance is the same as in the round optics, i.e. $\mu_{x/y} = 31.21\,/\,30.373$, where the nominal $DA_{\rm min/ave} = 10.56\,\sigma\,/\,13.19\,\sigma$, hence relatively close to the values for the round optics. The maximum $DA_{\rm min} =$

$11.86\,\sigma$ and $DA_{\text{ave}} = 13.52\,\sigma$ are achieved at $\mu_{x/y} = 30.98\,/\,29.82$, where the minimum DA is improved by more than $1\,\sigma$. Comparison of the nominal and the optimized DA is shown in Fig. 4.

One can see that although the same FQ is used for the round and flat collision optics, the resulting optimal phase settings are different. This is due to the substantial difference in the IP magnet's beta functions that act as amplification factors for the field error effects. Consequently, the effects of the IR1/5 field errors on the DA are different in the two optics resulting in different optimal phase settings.

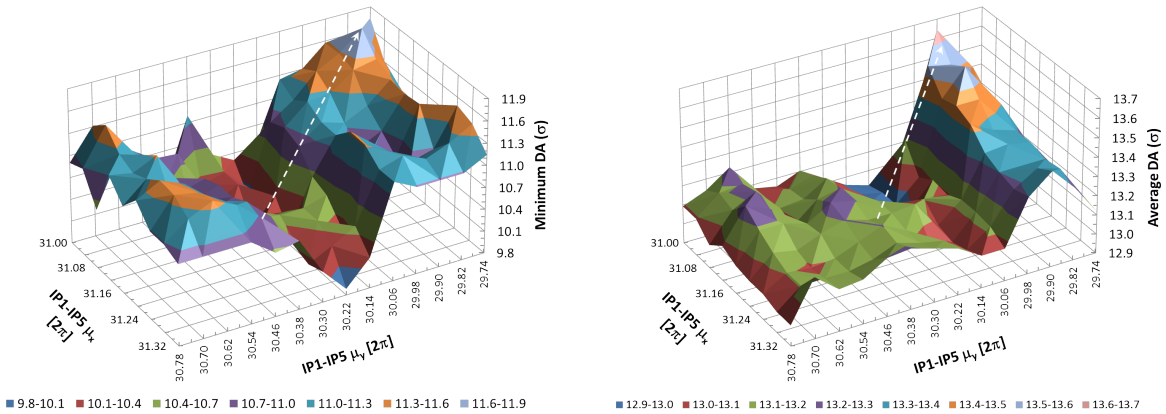

Fig. 3: Minimum (left) and average (right) DA of flat collision optics vs IP1-IP5 phase advance. The arrow connects the nominal and maximum DA.

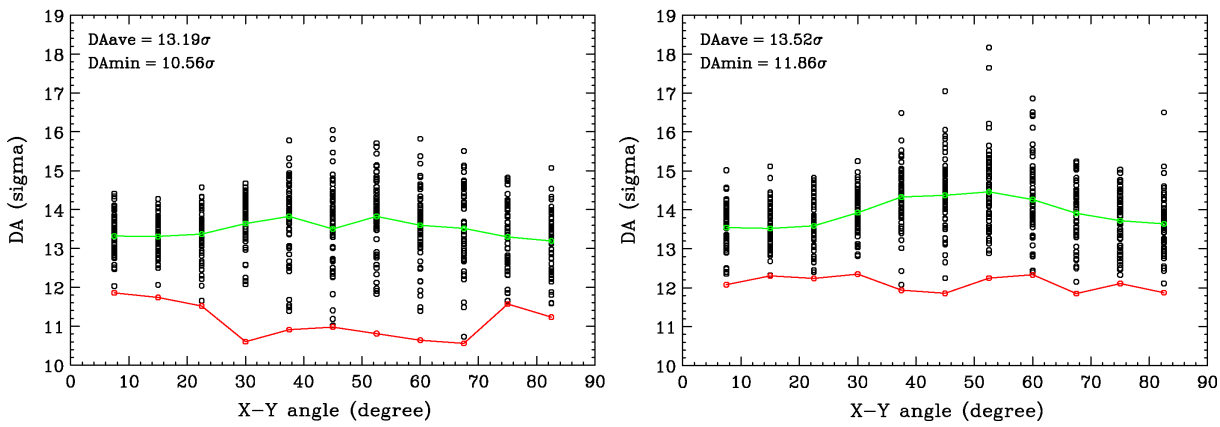

Fig. 4: DA of flat collision optics for the nominal (left) and optimized, using DA_{min}, (right) IP1-IP5 phase advance, where the circles represent the different seeds, and the green and red lines show the average and minimum DA at the 11 $x - y$ angles, respectively.

The DA scan for the injection optics is shown in Fig. 5. The nominal IP1-IP5 phase advance is $\mu_{x/y} = 31.195\,/\,30.368$, where the $DA_{\text{min/ave}} = 11.92\,\sigma\,/\,12.69\,\sigma$. The maximum $DA_{\text{min}} = 13.04\,\sigma$ and $DA_{\text{ave}} = 13.55\,\sigma$ are achieved at $\mu_{x/y} = 31.08\,/\,30.06$, where the minimum DA is improved by more than $1\,\sigma$. Comparison of the nominal and optimized DA is shown in Fig. 6.

The summary of the IP1-IP5 phase advance scans for the round, flat and injection optics is presented in Table 3. The optimisation procedure generates different optimal phase advance and DA values, depending on whether the minimum or average DA is selected as figure of merit for the optimisation process. It is worth noting that the round optics features the largest difference in terms of optimised

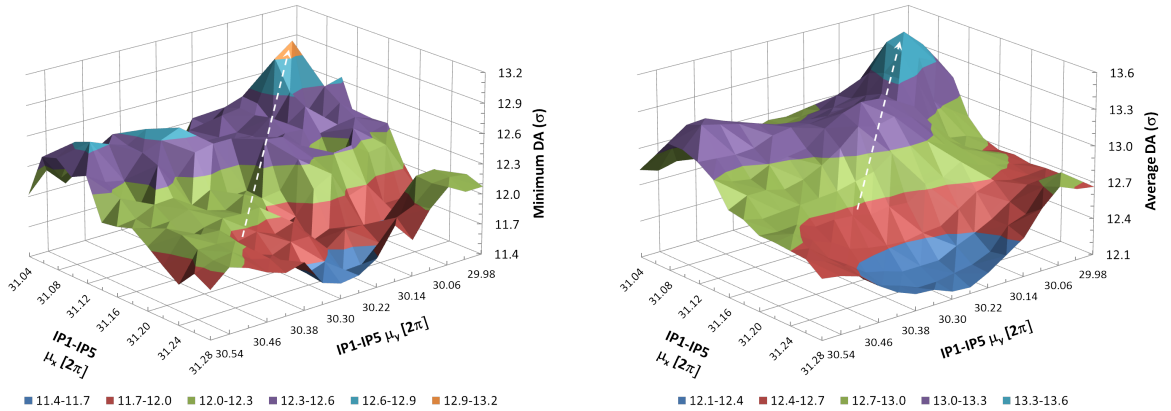

Fig. 5: Minimum (left) and average (right) DA of injection optics vs IP1-IP5 phase advance. The arrow connects the nominal and maximum DA.

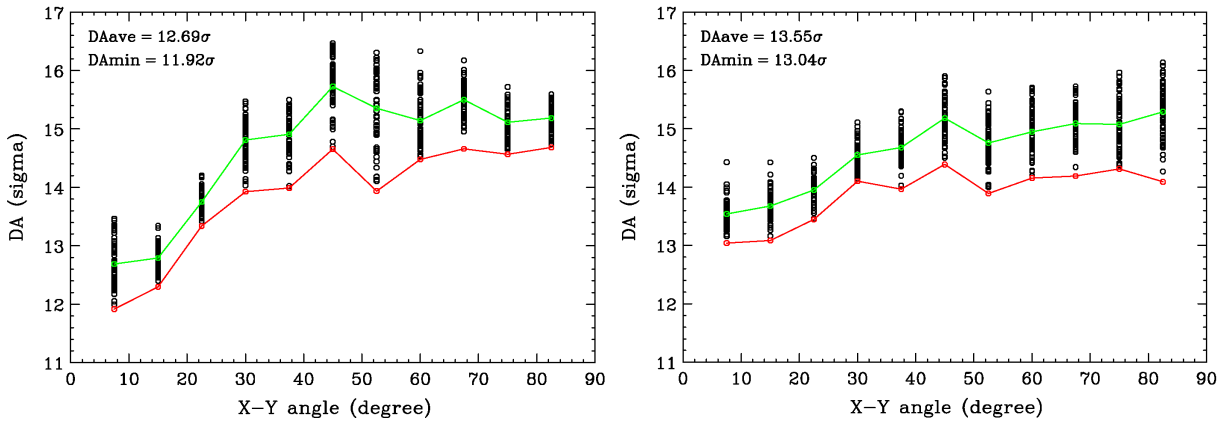

Fig. 6: DA of injection optics for the nominal (left) and optimized, using $DA_{\min}$, (right) IP1-IP5 phase advance, where the circles represent the different seeds, and the green and red lines show the average and minimum DA at the 11 $x-y$ angles, respectively.

DA depending on the figure of merit applied for the optimisation. The flat optics features smaller variations in the optimised DA values. On the other hand, the injection optics is insensitive to the type of optimisation (average or minimum DA) carried out. This might be linked to the fact while the injection optics does not feature any dominating error, the collision optics, round or flat, enhance the relevance of the IT FQ and of D1, and D2 separation dipoles over the rest of the machine. Figure 7 shows the DA when the Landau octupoles are set to the strength of -570 A and -20 A at collision and injection energies, respectively. In this case the octupole effects dominate the global dynamics and, although the optimized phase advance still improves the DA, a new phase-advance optimization should be attempted in these conditions. It is worth noting that since the DA optimization of the collision optics is the result of improving the compensation of the IP1 and IP5 non-linear field errors, the optimal IP1-IP5 phase advance is sensitive to the FQ of the IR1/5 magnets. Hence, in case of a non-negligible change of FQ the optimization needs to be revised.

Table 3: Nominal and optimized IP1-IP5 phase advance and corresponding dynamic aperture for the round and flat collision optics and the injection optics. The optimisation is performed on the minimum dynamic aperture and the Landau octupoles are switched off and $Q' = +3$.

Optics	Round	Flat	Injection
Nominal $\mu_{x/y}$ $[2\pi]$	31.210 / 30.373	31.210 / 30.373	31.195 / 30.368
Optimized (DA_{min}) $\mu_{x/y}$ $[2\pi]$	31.280 / 30.020	30.980 / 29.820	31.080 / 30.060
Optimized (DA_{ave}) $\mu_{x/y}$ $[2\pi]$	31.140 / 29.900	31.000 / 29.900	31.080 / 30.060
Nominal min/ave DA $[\sigma]$	10.30 / 13.18	10.56 / 13.19	11.92 / 12.69
Optimized (DA_{min}) min/ave DA $[\sigma]$	12.33 / 14.18	11.86 / 13.52	13.04 / 13.55
Optimized (DA_{ave}) min/ave DA $[\sigma]$	11.62 / 14.60	11.57 / 13.64	13.04 / 13.55

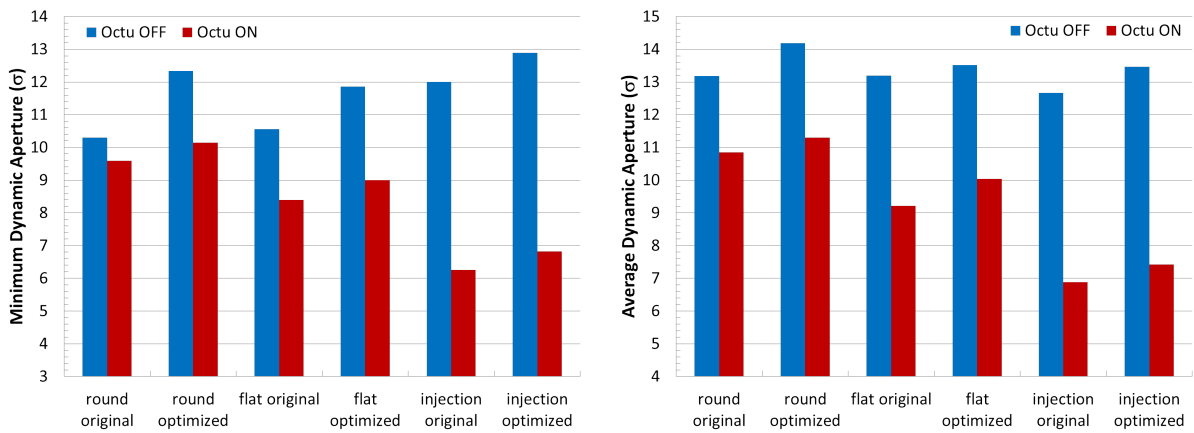

Fig. 7: Minimum (left) and average (right) DA before and after optimization of IP1-IP5 phase advance for the round, flat and injection optics. Two options are shown for the Landau octupoles, namely turned off (blue) and at nominal strength (red), corresponding to -570 A and -20 A at collision and injection energies, respectively.

4 DA and betatron tune

4.1 Collision and injection

The HL-LHC optics V1.0 uses the same fractional betatron tunes as in the LHC, namely $0.31 \,/\, 0.32$ (x/y) at collision and $0.28 \,/\, 0.31$ at injection. Due to the FQ of the new magnets and the new IR1/5 low-beta optics, it is possible that in HL-LHC the effects of non-linear resonances driven by the IR1/5 field errors may have changed with respect to LHC, thus affecting differently the DA. It is therefore logical to verify whether the current nominal working point is still the optimal one, and if there are alternative tune choices where the DA is larger. In this study we perform dynamic aperture tune scans for the round collision and injection optics, where the optimal IP1-IP5 phase advances from the previous study and the IT FQ in Table B.2 are used, and the Landau octupoles are turned off. It is important to note that the results of this study are only applicable to the beam without collision since beam-beam effects are not included in the simulations. These effects, however, play a significant role in the choice of the optimal tunes.

Results of the DA tune scan for the round collision optics with the optimized IP1-IP5 phase advance are presented in Fig. 8, where the minimum (left) and average (right) DA are shown. Dynamic aperture at the nominal tune of $Q_{x/y} = 62.31 \,/\, 60.32$ is $DA_{\text{min/ave}} = 12.33\,\sigma \,/\, 14.18\,\sigma$. The scan shows that the nominal tune is close to the local maximum DA, and therefore is still a valid choice. The scan also finds another local maximum for the DA at $Q_{x/y} = 62.27 \,/\, 60.28$, where

$DA_{\mathrm{min/ave}} = 13.13\,\sigma\,/\,14.28\,\sigma$, which is somewhat larger than the nominal DA value. Figure 9 shows the nominal and alternative tunes on the working point diagram together with the resonance lines up to the 8th order. A detailed comparison of the DA of round collision optics at these tunes is shown in Fig. 10.

Note that the alternative tune is located farther away from the 3rd order resonances, but closer to the 4th order ones. Since the scan is performed with the octupoles turned off, it is important to verify whether the proximity to the 4th order resonances driven by octupoles has an impact on the DA when the Landau octupoles are turned on. In addition, we verify the DA at the alternative tune for the large operational linear chromaticity of up to $+20$ units. The results are presented in Fig. 11. The DA dependence on chromaticity at the alternative tune is comparable to that at the nominal tune, although the minimum DA is considerably improved. However, the DA reduction with the octupole strength is noticeably faster at the alternative tune, resulting in about $2\,\sigma$ smaller DA at the nominal octupole strength as compared to the configuration with the nominal tune. We therefore conclude that the nominal tune is still the optimal choice for the round collision optics. Furthermore, based on the LHC experience, this tune is also favoured from the beam-beam point of view.

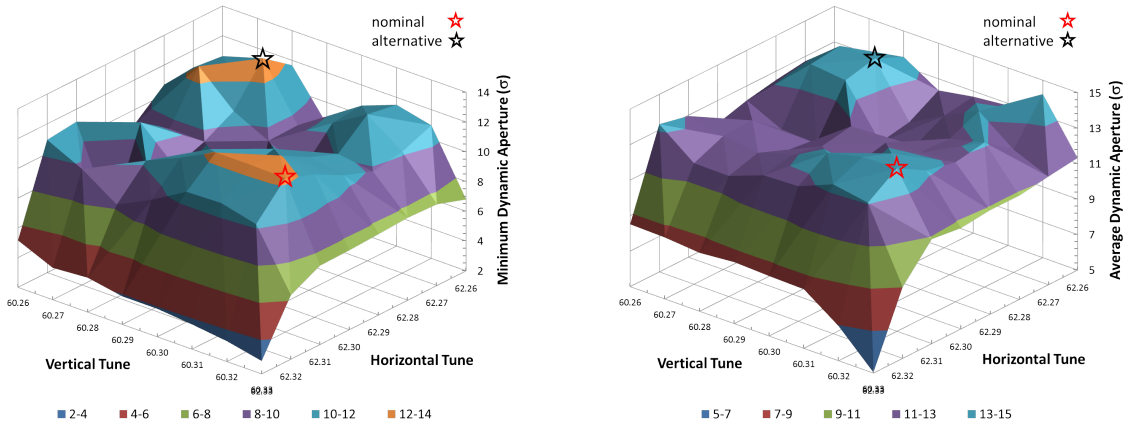

Fig. 8: Minimum (left) and average (right) DA of round collision optics vs betatron tunes, for the optimized value of the IP1-IP5 phase advance. The stars indicate the DA at the nominal (red) and the alternative (black) tunes.

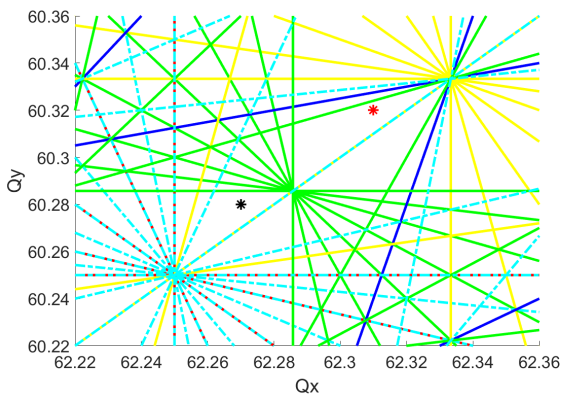

Fig. 9: The nominal (red star) and alternative (black star) tunes for round collision optics on the tune diagram with resonance lines up to the 8th order.

The DA tune scan for the injection optics with the optimized IP1-IP5 phase advance is shown in

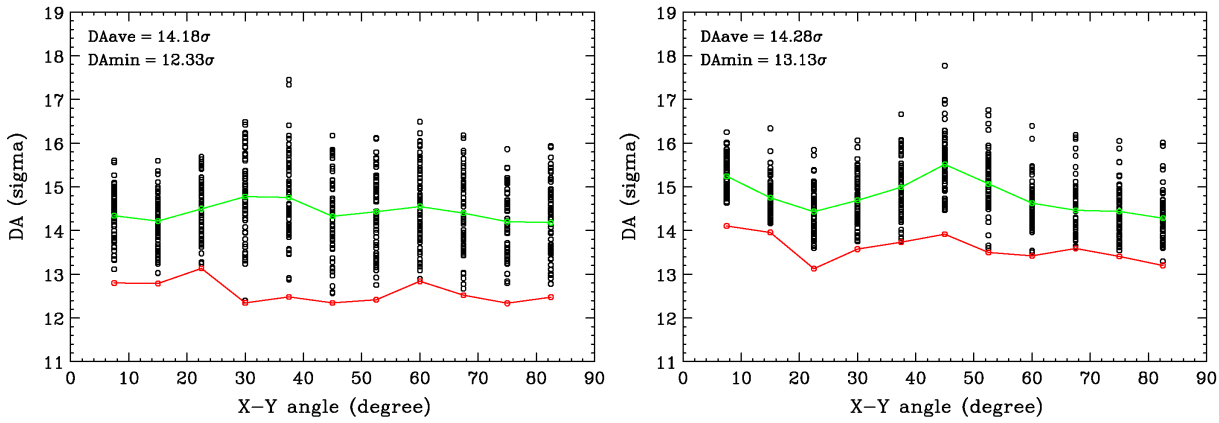

Fig. 10: DA of round collision optics for the nominal (left) and alternative (right) betatron tunes, where the circles represent the different seeds, and the green and red lines show the average and minimum DA at the 11 $x - y$ angles, respectively. The IP1-IP5 phase advance is optimized.

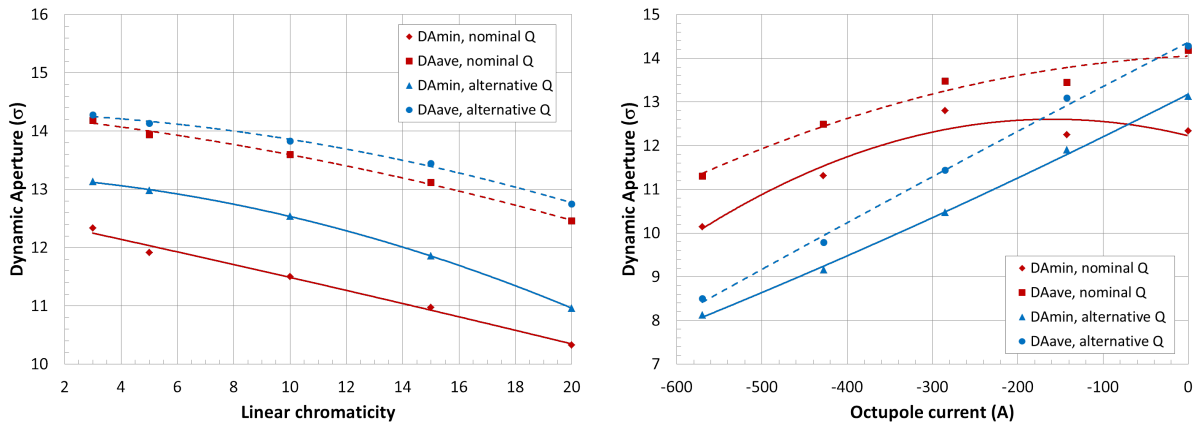

Fig. 11: DA of round collision optics vs chromaticity (left plot, where octupoles are turned off) and vs octupole current (right plot, where linear chromaticity is +3) at the nominal and alternative tunes. The IP1-IP5 phase advance is optimized. The lines represent polynomial fit of order 2.

Fig. 12. Dynamic aperture at the nominal tune of $Q_{x/y} = 62.28\,/\,60.31$ is $DA_{\mathrm{min/ave}} = 13.04\,\sigma\,/\,13.55\,\sigma$. Similarly to the collision scan, the injection one confirms that the nominal tune is still a good choice, since it is located at the local maximum of the DA. The scan also finds another local maximum for the DA at $Q_{x/y} = 62.31\,/\,60.29$, where $DA_{\mathrm{min/ave}} = 13.28\,\sigma\,/\,14.22\,\sigma$, which is somewhat larger than the nominal value. Figure 13 shows the nominal and alternative tunes on the tune diagram with the resonance lines up to the 8th order. A detailed comparison of the injection DA at these tunes is shown in Fig. 14.

We verify also the DA sensitivity at the nominal and alternative injection tunes to the large operational chromaticity and octupole strength. The results are presented in Fig. 15. They show that at the alternative tune the injection DA is somewhat more sensitive to the chromaticity, although it is less affected by the octupole strength than at the nominal tune. The latter may be due to a better location of the alternative tune relative to the 4th order resonances. However, a possible complication is that the alternative tune is located on the other side of the $Q_x = Q_y$ resonance with respect to the collision tune. Therefore, transition from injection to collision would require crossing this coupling resonance. Taking this into account, we conclude that the nominal injection tune appears optimal also for the HL-LHC. The

summary of the tune scans results for the round collision and injection optics is presented in Table 4.

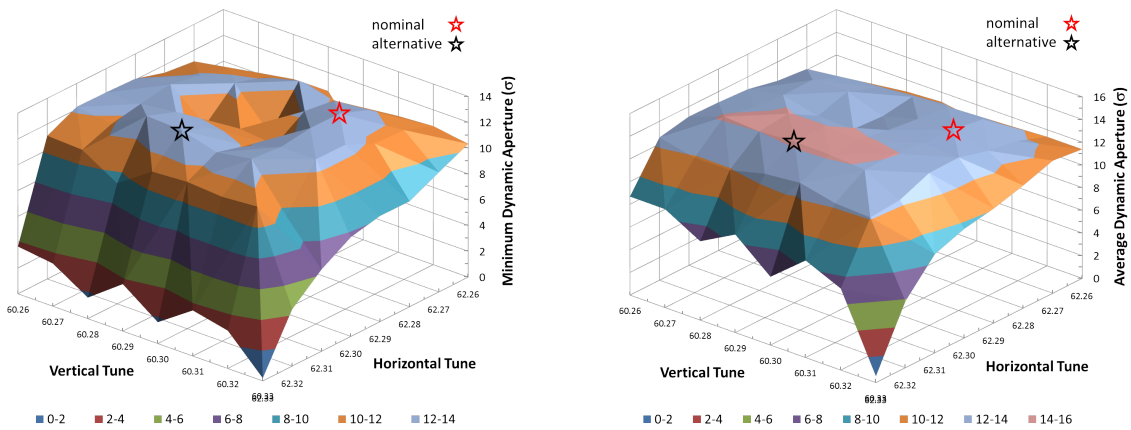

Fig. 12: Minimum (left) and average (right) DA of injection optics vs betatron tune, where the IP1-IP5 phase advance is optimized. The stars indicate the DA at the nominal (red) and the alternative (black) tunes.

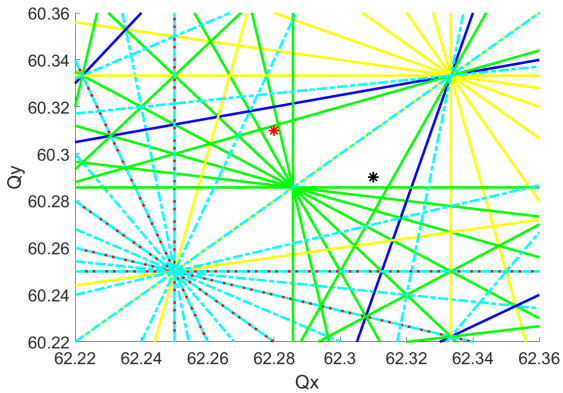

Fig. 13: The nominal (red star) and alternative (black star) tunes for injection optics on the tune diagram with resonance lines up to the 8th order.

4.2 Pre-squeeze

In HL-LHC, the transition from injection optics to pre-collision optics is planned to be done during the energy ramp. In this process, called pre-squeeze, the IP1/5 β^* is reduced from 6 m to 0.64 m and the energy is increased from 450 GeV to 7 TeV. The injection betatron tunes ($Q_{x/y} = 62.28 \,/\, 60.31$) must be changed to the collision ones (62.31 / 60.32) during such a tune-change process. In this study, we investigate the optimal β^* at which this tune transition should be performed.

The goal is to preserve the maximum DA during the whole pre-squeeze process. Several factors affect the DA in this stage: 1) the reduction of β^* increases the values of the beta functions at the IT, D1, and D2 magnets, thus enhancing the effects of their magnetic field errors; 2) the magnets FQ varies with beam energy, thus changing the impact of field errors; 3) the beam size scales with energy E as $\sigma \propto 1/\sqrt{E}$, which changes the DA size in terms of the number of beam's σ.

To investigate the optimal choice of β^* value at which the tunes should change, we perform tracking simulations to scan the DA with β^* in the range from 2.9 m to 0.7 m for both injection and collision

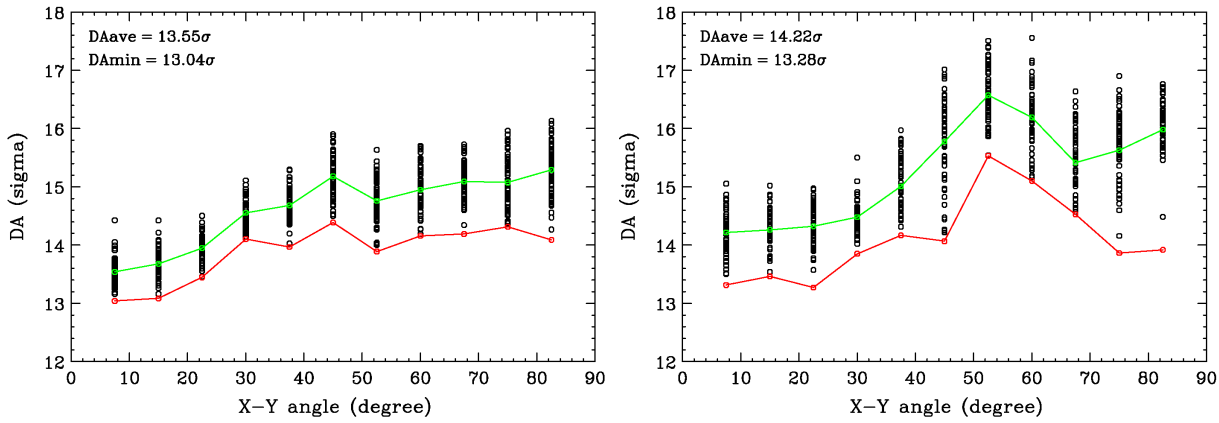

Fig. 14: DA of injection optics for the nominal (left) and alternative (right) betatron tunes, where the circles represent the different seeds, and the green and red lines show the average and minimum DA at the 11 $x - y$ angles, respectively. The IP1-IP5 phase advance is optimized.

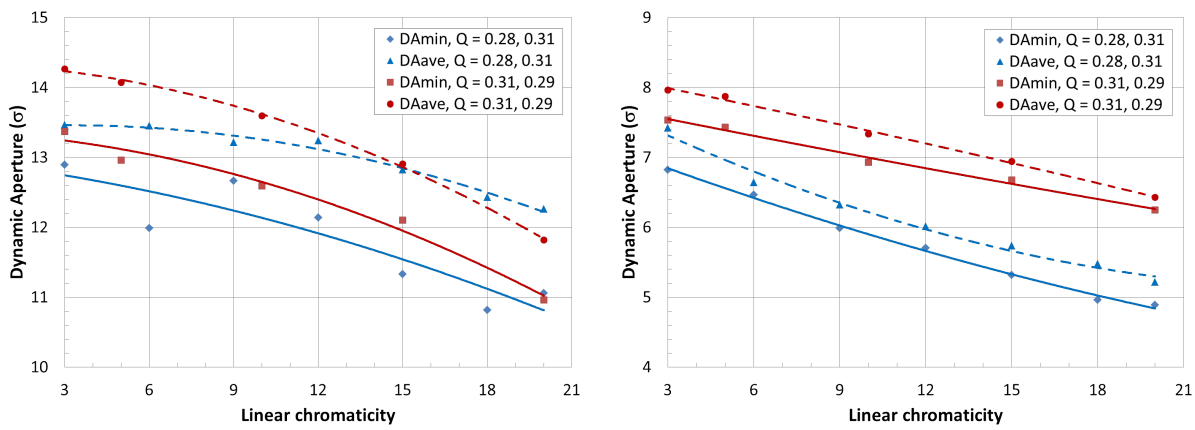

Fig. 15: DA of injection optics at the nominal and alternative tunes for two options of the Landau octupoles, namely turned off (left) and set to the nominal strength of -20 A (right). The IP1-IP5 phase advance is optimized. The lines represent polynomial fit of order 2.

tunes. Note that this range corresponds approximately to the second half of the pre-squeeze. Since the energy changes along with β^*, ideally the magnet FQ should also continuously change during the numerical scan. However, due to lack of detailed knowledge of FQ dependence on beam energy, the calculations are performed only for two FQ settings corresponding to 450 GeV and 7 TeV energy. This implies that the results obtained with 7 TeV FQ are more realistic for lower values of β^* whereas the results with 450 GeV FQ are more relevant at higher values of β^*. The IT FQ in Tables B.3, B.4 is used in the study, which includes also the separate contribution of the IT quadrupole end fields. To express the DA in terms of the number of σ, we calculate the beam σ assuming that β^* is changed linearly with beam energy, where β^* and E ranges are taken from 6 m to 0.64 m and from 450 GeV to 7 TeV, respectively.

The results are presented in Fig. 16 for the case of low ($+3$, upper row) or high ($+20$, lower row) Q'. Note that the upper left plot in Fig. 16 also includes the points from the collision range at $\beta^* < 0.64$ m. One can observe that in the studied range, the collision tunes yield a larger DA for both the 7 TeV and 450 GeV FQ. The only exception is the case of $Q' = +20$ and 450 GeV FQ shown in the lower right plot of Fig. 16, where the DA for injection tunes is larger at $\beta^* < 1$ m. For this β^* value,

Table 4: The nominal and alternative betatron tunes and dynamic aperture for the round collision and injection optics, where the IP1-IP5 phase advance is optimized and the Landau octupoles are switched off and $Q' = +3$.

Optics	Round Collision	Injection
Nominal $Q_{x/y}$	62.31 / 60.32	62.28 / 60.31
Alternative $Q_{x/y}$	62.27 / 60.28	62.31 / 60.29
Nominal min/ave DA $[\sigma]$	12.33 / 14.18	13.04 / 13.55
Alternative min/ave DA $[\sigma]$	13.13 / 14.28	13.28 / 14.22

however, the beam energy is high enough, so the result using 7 TeV FQ (lower left plot in Fig. 16) should be more accurate, and there the DA at collision tunes is larger.

Based on these results, we conclude that for $\beta^* < 3$ m the DA at collision tunes exceeds that for injection tunes. Therefore, for the sake of preserving the DA, the transition from injection to collision tunes should occur during the first half of the pre-squeeze, i.e. for $3\,\mathrm{m} < \beta^* < 6\,\mathrm{m}$.

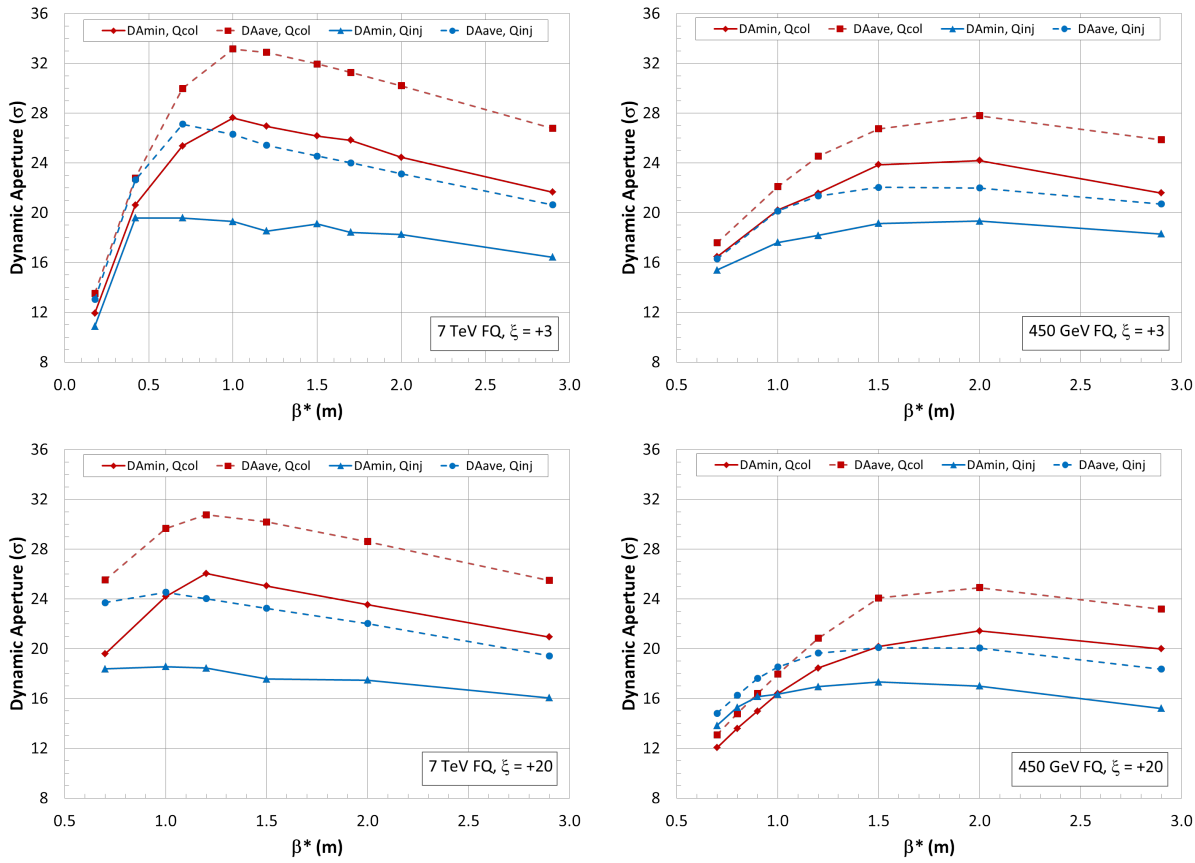

Fig. 16: Upper: DA during the second part of the pre-squeeze ($\beta^* < 3$ m) at collision (red) and injection (blue) tunes for IT FQ at 7 TeV (left) and 450 GeV (right), and $Q' = +3$. Lower: DA during the second part of the pre-squeeze ($\beta^* < 3$ m) at collision (red) and injection (blue) tunes for IT FQ at 7 TeV (left) and 450 GeV (right), and $Q' = +20$. The beam size is scaled with energy as $\sigma \propto 1/\sqrt{E}$.

5 DA for various operational conditions

Attaining the optimal beam quality in operation and satisfying a variety of experimental conditions may require adjustment of the lattice parameters over a broad range of values. Below we discuss the impact of such adjustments on the DA, including variation of the IP1/5 beta function, the linear chromaticity, and the strengths of the Landau octupoles.

The DA of the round collision optics as a function of β^* for a range of chromaticity values from $+2$ to $+18$ is shown in Fig. 17. In this simulation, the beam energy is 7 TeV, the IT FQ as reported in Table B.2 is used, the Landau octupoles are off, and the beam separation at IP1/5 is ± 0.75 mm. One can see that the DA notably improves even with a small increase of β^*, gaining roughly $1\,\sigma$ for every 2 cm of β^*. This provides an operational flexibility for adjustment of the beam lifetime with a mild degradation of instantaneous luminosity. The slightly quadratic dependence of DA with β^* may be explained by the fact that as the DA increases, the non-linear field due to errors increases more rapidly at large amplitude, thus limiting the DA. The reduction of the DA due to large Q' is up to $2\,\sigma$ at low β^* and somewhat increases at higher β^*. The latter, however, is not of concern since the DA is large in the high β^* range.

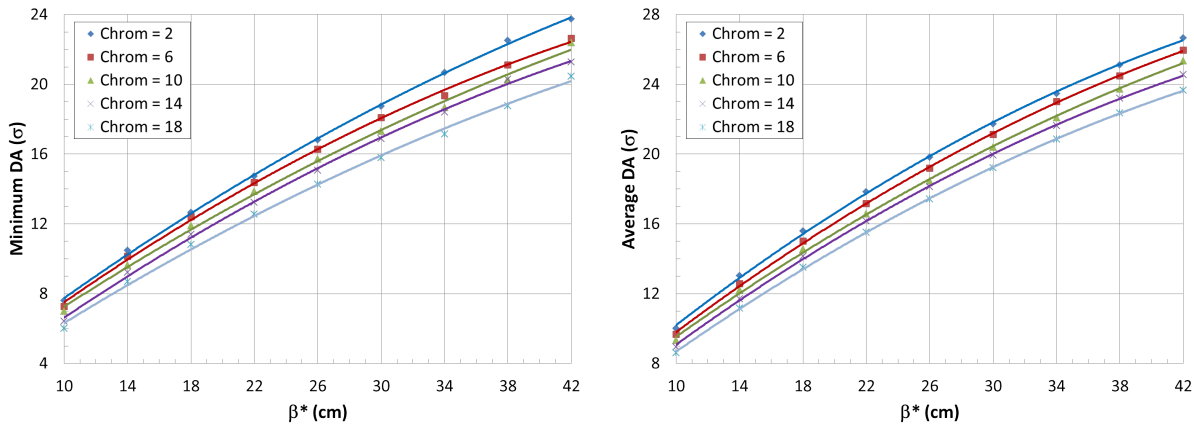

Fig. 17: Minimum (left) and average (right) DA of round collision optics vs β^* and linear chromaticity. The lines represent polynomial fit of order 2.

The dependence of DA at injection on chromaticity is presented in Fig. 18 (left), where two options are included, namely with Landau octupoles turned off and set to the nominal current of -20 A. These results are obtained with the IT FQ of Table B.4 and injection optics with the optimized IP1-IP5 phase advance. Similarly to the collision optics, the DA reduction at large chromaticity of $+20$ is about $2\,\sigma$. A much stronger impact on the DA is due to the octupoles, which amounts to about $6\,\sigma$ reduction at -20 A, where the DA is nearly $7\,\sigma$ at the nominal chromaticity of $+3$, and only $5\,\sigma$ at the chromaticity of $+20$.

Operational experience with the LHC shows that at certain conditions the strength of Landau octupole at injection energy may need to be increased even further. Figure 18 (right) presents the HL-LHC DA at injection energy where the range of the octupole current is further extended to -40 A. With such strong octupoles, the DA is reduced to below $5\,\sigma$, which may not be sufficient for an adequate beam lifetime.

The impact of the octupole strength on the collision DA is presented in Fig. 19, where the nominal octupole current is -570 A. The simulations include both the round (left) and flat (right) collision optics, where the IP1-IP5 phase advance is optimized, the 7 TeV IT FQ in Table B.2 is used. One can see that the impact of the nominal octupole strength is a reduction of about $2\,\sigma$ of the DA, which is, however, still above $10\,\sigma$. A slightly stronger impact is observed on the flat optics, where the DA approaches $9\,\sigma$ at the nominal octupole current.

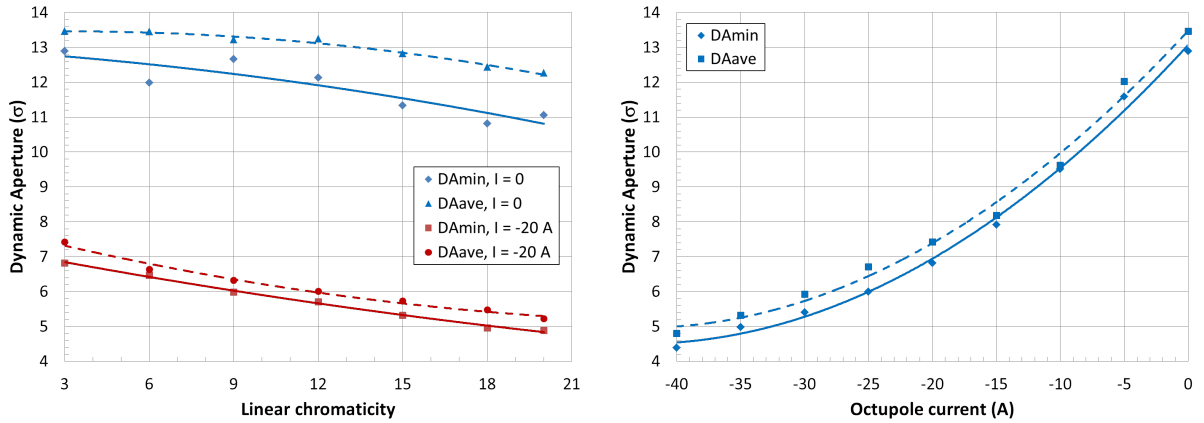

Fig. 18: Left: Minimum and average DA of injection optics vs chromaticity for two options of Landau octupoles, namely turned off (blue) and set to the nominal current of -20 A (red). Right: Minimum and average DA of injection optics vs octupole strength for a large range of octupole current up to -40 A. The IP1-IP5 phase advance is optimized and $Q' = +3$. The lines represent polynomial fit of order 2.

Finally, Fig. 20 shows the impact of strong octupoles on the DA of round collision optics during the beta squeeze, with $E = 7$ TeV. One can see that in the range of low β^* the rate of the DA change with β^* is about the same, no matter the value of the octupole strength. However, at the higher end of the β^* range the strong octupoles cause the DA to saturate more rapidly. This is due to the fact that the octupole field quickly increases as the third power of amplitude, thus becoming a limiting factor for the DA growth. In this range of the beta squeeze, however, the DA is quite large, so the impact of octupoles is not expected to be a source of significant concern for the beam lifetime.

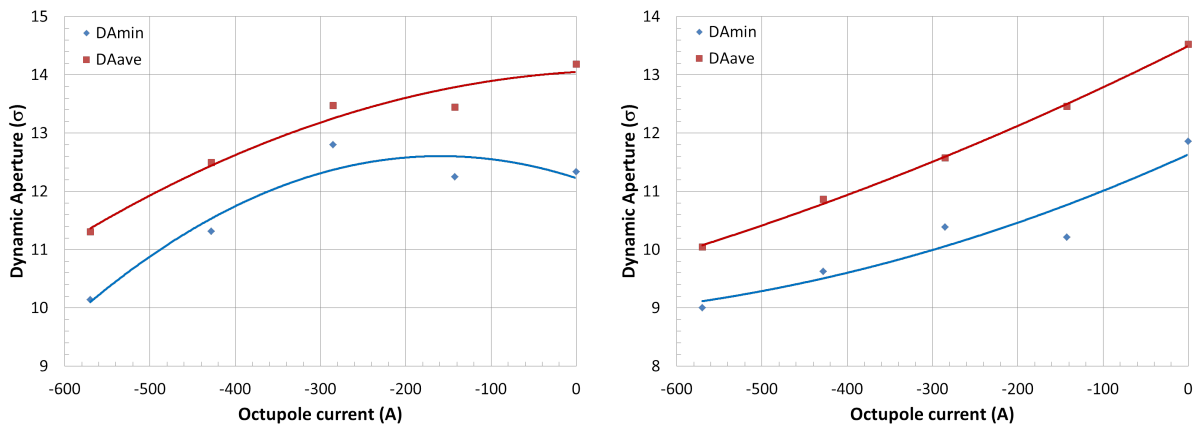

Fig. 19: Minimum and average DA of round (left) and flat (right) collision optics vs octupole strength. The IP1-IP5 phase advance is optimized.

6 DA with large triplet quadrupole field errors

Several short-model magnets of the IT quadrupoles have been built and measured. The measurements reveal that some field components significantly (a few times) exceed their expected range based on the specifications in Tables B.3, B.4, namely the a_3, b_3, a_4 and b_5 [13]. Magnetic shimming may be used to compensate the a_3 and b_3 [14]. However, the capability of such a method to correct the large a_4 and b_5

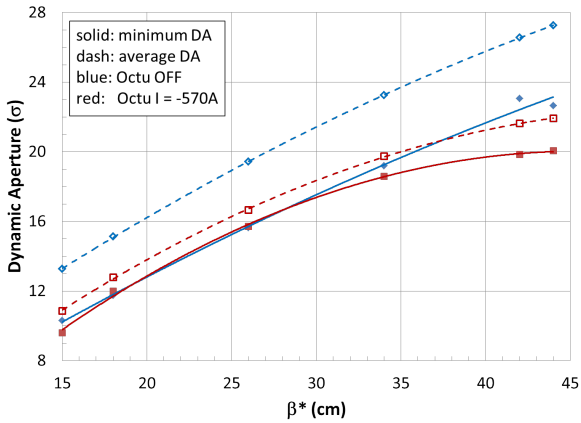

Fig. 20: DA of round collision optics vs β^* for two options of Landau octupoles, namely turned off and set to the nominal strength of -570 A.

is more limited, since it also affects the lower-order field components. It is possible that these errors will remain large in the final magnets or, at least, in a part of them. Therefore, it is essential to examine the capability of the IT corrector system, as currently specified, to compensate these large errors, as well as to evaluate their impact on dynamic aperture.

6.1 a_4 and b_5 errors

The IT FQ in Tables B.3, B.4 reports the following expected values, namely $a_{4\mathrm{U}} = a_{4\mathrm{R}} = 0.65$ and $b_{5\mathrm{U}} = b_{5R} = 0.42$. Based on these values and the expected error distribution in Eq. (3), the maximum possible absolute values of these errors are $a_{4\mathrm{max}} = a_{4\mathrm{U}} + 3a_{4\mathrm{R}} = 2.6$ and $b_{5\mathrm{max}} = b_{5\mathrm{U}} + 3b_{5\mathrm{R}} = 1.68$. The measurements of the IT model magnets, however, show that the actual a_4 and b_5 are as large as 6.5 and 3.2, respectively [13], which are up to a factor of 2.5 larger than the expectations. Since the origin of these errors is not completely understood and they cannot be efficiently corrected with magnetic shimming [14], it is possible that these errors will remain large in the final built magnets.

To evaluate the impact of the larger-than-expected a_4 and b_5 on the strength of the corresponding IT correctors and DA, including sufficient margin, tracking simulations are performed where these errors are increased up to a factor of $6-7$ relative to the expectations. The condition of $a_{4\mathrm{U}} = a_{4\mathrm{R}}$ and $b_{5\mathrm{U}} = b_{5\mathrm{R}}$ is maintained in all the cases. Figure 21 presents the DA of round and flat collision optics at the nominal and larger a_4 and b_5 values, where the nominal IP1-IP5 phase advance is used. The larger errors are corrected using the corresponding IT correctors, whose strengths are not limited in the simulations. At $a_{4\mathrm{U,R}} = 2$ and $b_{5\mathrm{U,R}} = 1.5$, the DA degradation is about $0.5\,\sigma$ and $0.8\,\sigma$ for the round and flat optics, respectively. The minimum DA of the round optics is $9.7\,\sigma$, which is still close to an acceptable level, while it is $9.0\,\sigma$ for the flat optics. For larger field errors the DA reduces almost linearly, where the impact on the flat optics DA is stronger.

A detailed DA 2D scan vs a_4 and b_5 is presented in Fig. 22 for minimum (upper) and average (lower) DA for the round collision optics, where the IT corrector strengths are not limited. It shows that the impact on DA is relatively mild in the range of $a_{4\mathrm{U,R}} < 3$ and $b_{5\mathrm{U,R}} < 1.5$, while for larger errors the DA degradation is primarily due to the large b_5.

The DA of the round collision optics with large a_4 and b_5 has been evaluated with the IP1-IP5 phase advance which was previously optimized for the nominal IT FQ. The resulting DA improvement is much smaller than in the case with the expected FQ. Clearly, the large a_4 and b_5 significantly alter the self-compensation of the IP1 and IP5 field errors, so the previously optimized phase advance is no longer valid. Consequently, the phase advance optimization should be redone for any non-negligible changes of

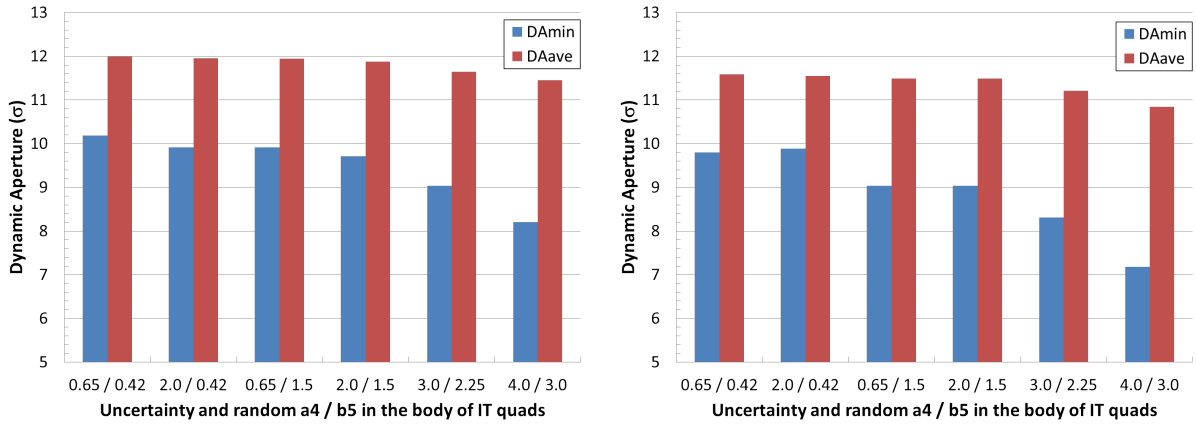

Fig. 21: DA of round (left) and flat (right) collision optics with large uncertainty and random a_4 and b_5 of the IT FQ.

the IT FQ.

The strength of the IT correctors depends linearly on the corresponding IT errors [4]. At present, the specified maximum strengths of the a_4 and b_5 correctors are 0.046 Tm and 0.025 Tm at $R_{\rm ref} = 50$ mm, respectively [4]. Figure 23 (left) shows the maximum IT corrector strengths in round collision optics in typical DA simulations with 60 seeds for the selected settings of the a_4 and b_5 errors, where the corrector strengths are not limited. From this figure, one can see that the maximum correctors strength quickly rise beyond their specification for the considered error range. The right-hand side plot of Fig. 23 shows the fraction of cases exceeding the specifications. It is worth noting that the distribution of correctors strength for 60 seeds has a tail where the correctors may reach rather large strength. For instance, in case of $b_{5\rm U,R} = 1.5$ there are only 3.3% of the out-of-spec b_5 correctors, however they exceed the specifications by up to 50%.

In view of the expected large a_4 and b_5 IT field errors, it is critical to examine the limitations of the present IT corrector specifications. Accordingly, one needs to determine the maximum required IT corrector strengths as a function of these errors. There are a total of 24 IT quadrupoles in the IR1 and 5 interaction regions, hence each simulation seed comprises 24 randomly-assigned a_4 (b_5) IT errors and four corresponding a_4 (b_5) correctors strength compensating these errors. Due to the random nature of the magnetic errors, the maximum corrector strength vs the errors may not be consistent from seed to seed. For instance, errors which add to each other may require a stronger corrector than larger errors which cancel each other, e.g. due to their signs. For this reason, we focus on more consistent quantities, namely the maximum corrector strength vs the maximum error obtained from a large number of seeds.

For high statistics, 600 seeds are generated for each setting of the pair of $a_{4\rm U,R}$ and $b_{5\rm U,R}$ in the simulations of the round collision optics. The maximum corrector strength is determined from the total of 2400 corrector strengths (4 correctors of each family per seed). To estimate the maximum error value in these simulations, we use a simplified method based on the error distribution in Eq. (3). It follows that for a very large number of seeds, the maximum absolute value of the a_4 and b_5 errors should approach the theoretically maximum values of $a_{4\rm max} = a_{4\rm U} + 3a_{4\rm R}$ and $b_{5\rm max} = b_{5\rm U} + 3b_{5\rm R}$, where the systematic terms are zero.

Figure 24 shows the maximum a_4 and b_5 correctors strength in the round collision optics versus the theoretically maximum $a_{4\rm max}$ and $b_{5\rm max}$ IT errors for two options of the D1 a_4 and b_5 errors, namely turned on and off, where the D1 specifications at 7 TeV are $a_{4\rm U,R} = 0.444$ and $b_{5\rm U,R} = 0.365$. The maximum correctors strength are normalized to their specification in this figure. Clearly, in this range of IT errors, the impact of the D1 field errors on the maximum IT corrector strength is negligible. The

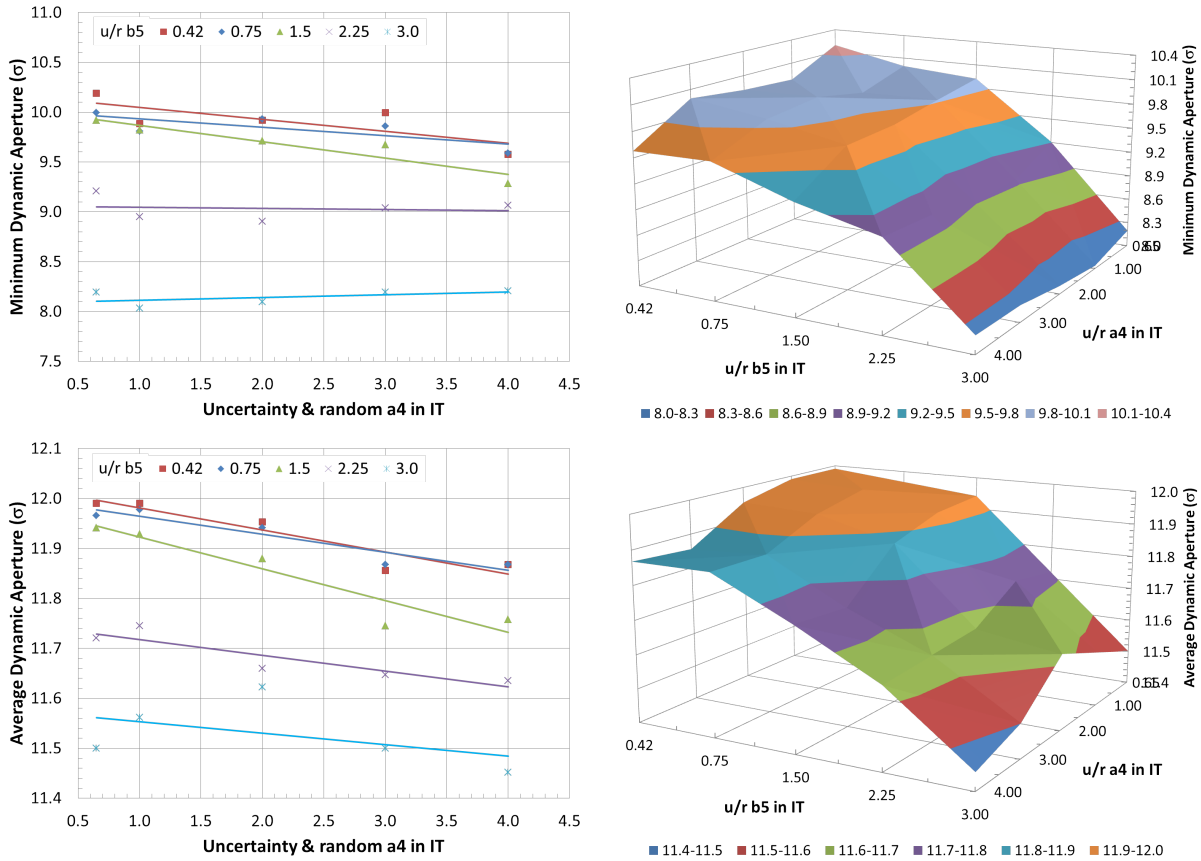

Fig. 22: Upper: Minimum DA of round collision optics vs uncertainty and random a_4 and b_5 of the IT FQ. Lower: Average DA of round collision optics vs uncertainty and random a_4 and b_5 of the IT FQ. 2D (left column) and 3D (right column) figures are shown.

maximum strength scales linearly with the maximum IT error except when the IT errors are close to zero, where the effect of the D1 errors starts to dominate. According to the linear fit, the present corrector specifications satisfy the maximum IT errors up to $a_{4\mathrm{max}} = 7.51$ and $b_{5\mathrm{max}} = 3.78$, which correspond to $a_{4\mathrm{U}} = a_{4\mathrm{R}} = 1.878$ and $b_{5\mathrm{U}} = b_{5\mathrm{R}} = 0.945$. These values fall comfortably within the range of $a_{4\mathrm{U,R}} < 3$ and $b_{5\mathrm{U,R}} < 1.5$, where the impact on the DA is mild as determined previously in Fig. 22. An example of the corrector strength distribution for the case $a_{4\mathrm{U}} = a_{4\mathrm{R}} = 2$ and $b_{5\mathrm{U}} = b_{5\mathrm{R}} = 1.5$ is shown in Fig. 25.

These results indicate that the present IT corrector specifications may be sufficient to compensate the large observed range of measured errors of up to $a_4 = 6.5$ and $b_5 = 3.2$, however with a considerably reduced margin of only 13%. Note also that due to the still limited statistics in the simulations, the obtained results should be considered optimistic, i.e. the maximum acceptable errors may be somewhat smaller, further reducing the margin. In these circumstances and in view of other unaccounted uncertainties, it is desirable to increase the corrector specification strengths. The feasible options [15] are longer correctors and/or higher operational current. As it is mentioned in the conclusions, suitable strength margins have been re-gained thanks to an increase in length of the non-linear correctors as of V1.4 layout.

Finally, we verify the impact of large a_4 and b_5 errors on the DA of injection optics. It was established before that for the nominal IT FQ, due to the relatively small beta function values at the ITs, the injection DA is not sensitive to the IT field errors, therefore the IT correctors are not used in this

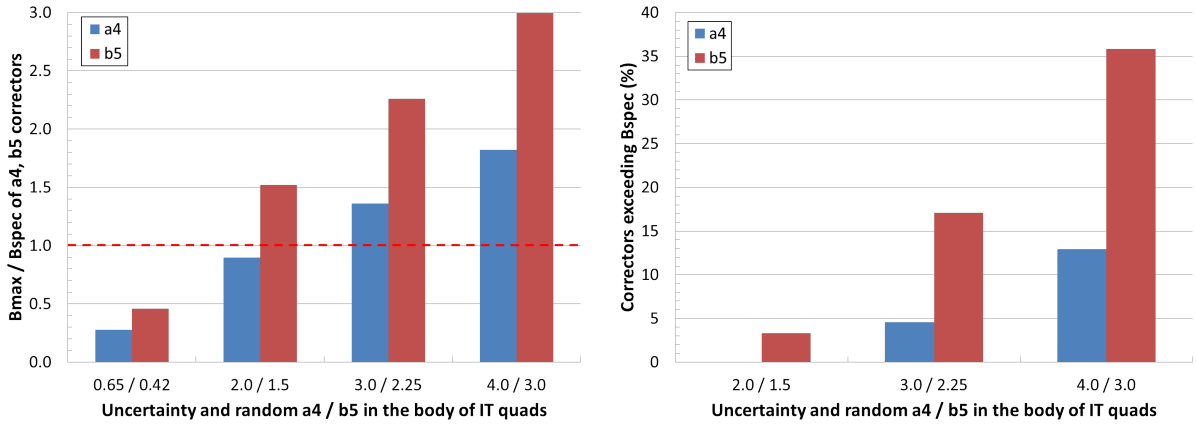

Fig. 23: Maximum strengths of the a_4 and b_5 IT non-linear correctors with large a_4 and b_5 IT errors (left) in the round collision optics, and the relative number of cases exceeding the specified maximum strengths (right). The dashed-red line in the left plot indicates the specification strength.

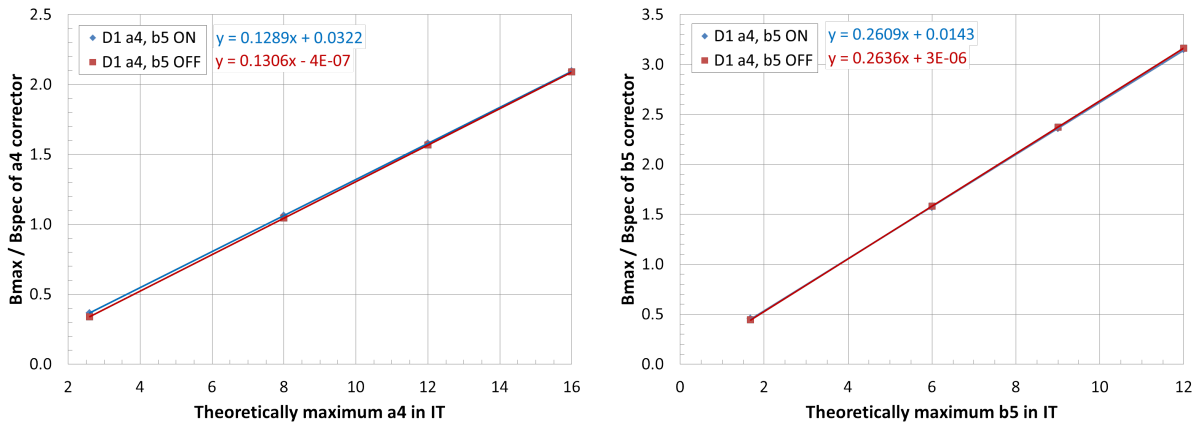

Fig. 24: Maximum normalized strengths of the IT a_4 and b_5 correctors in the round collision optics vs the theoretically maximum a_4 and b_5 errors in the IT quadrupoles, where the a_4 and b_5 errors in the D1 dipoles are turned on (blue) or off (red).

optics. The results of the DA simulations with the larger errors are presented in Fig. 26. The plot on the left shows that the DA is still not much affected even at the largest errors, therefore the large measured errors are acceptable at injection energy. The right-hand side plot presents the DA comparison for the nominal (left) and the previously optimized (right) IP1-IP5 phase advance. One can observe that the optimization is still valid with the larger errors, providing nearly the same improvement of the injection DA as at the nominal IT FQ.

6.2 a_3 and b_3 errors

The IT FQ in Tables B.3, B.4 specifies the third order multipoles: $a_{3\mathrm{U}} = a_{3\mathrm{R}} = 0.65$ and $b_{3\mathrm{U}} = b_{3\mathrm{R}} = 0.82$. Based on the error distribution in Eq. (3), these expected values correspond to the theoretically maximum random errors of $a_{3\mathrm{max}} = 2.6$ and $b_{3\mathrm{max}} = 3.28$. Field measurements, however, show a larger spread of these errors in the IT model magnets [13]. As pointed out [13], a magnetic shimming can be used to compensate these low order errors. Nonetheless, we assume here a pessimistic scenario

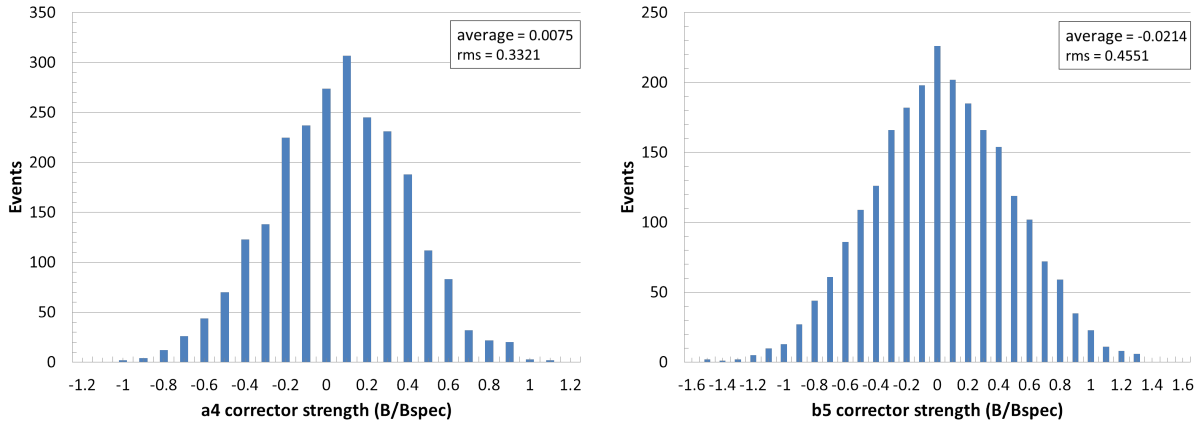

Fig. 25: Normalized strengths of the IT a_4 (left) and b_5 (right) correctors in 600 seeds for the round collision optics, where $a_{4\mathrm{U,R}} = 2$ and $b_{5\mathrm{U,R}} = 1.5$ in the IT quadrupoles and the D1 a_4 and b_5 errors are included.

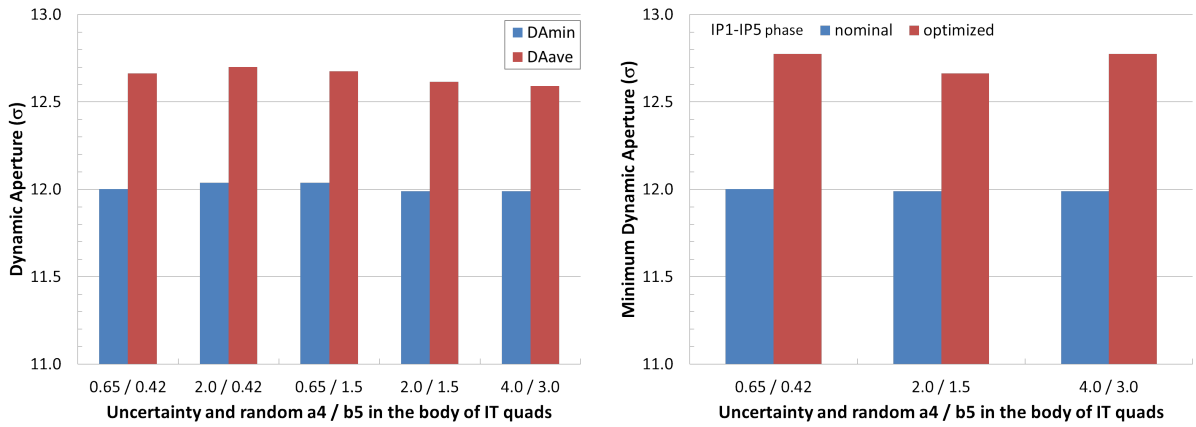

Fig. 26: DA of injection optics vs uncertainty and random a_4 and b_5 of the IT FQ with the nominal IP1-IP5 phase advance (left) and the improvement of the minimum DA with the optimized IP1-IP5 phase advance (right). The IT non-linear field correctors are off.

and investigate the situation where these errors are very large, i.e. up to $6 - 7$ times larger than the expected values.

Analogous to the study of the a_4 and b_5 errors, tracking simulations with 600 seeds are performed to evaluate the maximum strengths of the a_3 and b_3 IT correctors versus the theoretically maximum a_3 and b_3 IT errors. The round collision optics with the nominal IP1-IP5 phase advance is used and the IT corrector strengths are not limited. The condition $a_{3\mathrm{U}} = a_{3\mathrm{R}}$ and $b_{3\mathrm{U}} = b_{3\mathrm{R}}$ is maintained while the errors are increased.

The results are presented in Fig. 27 for two options of the a_3 and b_3 errors in the D1, namely turned on and off, where the D1 specifications at 7 TeV are $a_{3\mathrm{U,R}} = 0.282$, $b_{3\mathrm{S}} = -0.9$ and $b_{3\mathrm{U,R}} = 0.727$. The maximum correctors strength in Fig. 27 are normalized to their nominal values of 0.063 Tm at $R_{\mathrm{ref}} = 50$ mm radius [4]. The impact of the D1 errors on the maximum IT correctors strength is practically negligible, except when the IT errors are close to zero. According to the linear fit, the present correctors specification are compatible with $a_{3\mathrm{max}} = 6.32$ and $b_{3\mathrm{max}} = 9.17$, which correspond to

$a_{3\mathrm{U,R}} = 1.58$ and $b_{5\mathrm{U,R}} = 2.29$. The latter exceeds the specifications in Table B.3 by a factor of $2.4 - 2.8$. An example of the corrector strength distribution for the case of $a_{3\mathrm{U,R}} = 2$ and $b_{3\mathrm{U,R}} = 3$ is shown in Fig. 28.

These results indicate that the current a_3 and b_3 corrector specifications are sufficient for the observed maximum measured errors of $a_3 = 3.3$ and $b_3 = 4.2$ [13] since the latter is a factor of two smaller than the acceptable values determined above. As mentioned before, due to the still limited statistics in the simulations and the small sample of results from magnetic measurements, the results should be considered optimistic, i.e. the actual acceptable maximum errors may be somewhat smaller.

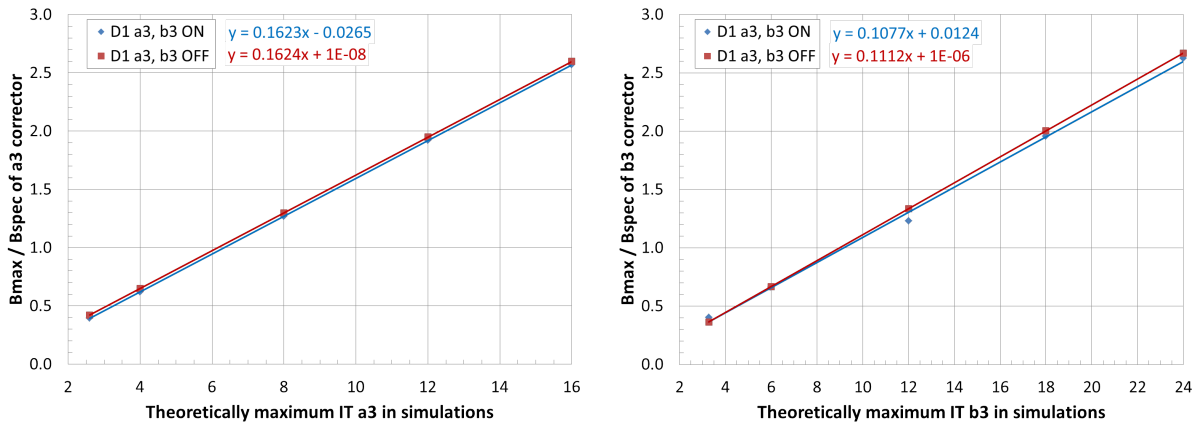

Fig. 27: Maximum normalized strengths of the IT a_3 and b_3 correctors in the round collision optics vs the theoretically maximum a_3 and b_3 errors in the IT quadrupoles, where the a_3 and b_3 errors in the D1 dipoles are turned on (blue) or off (red).

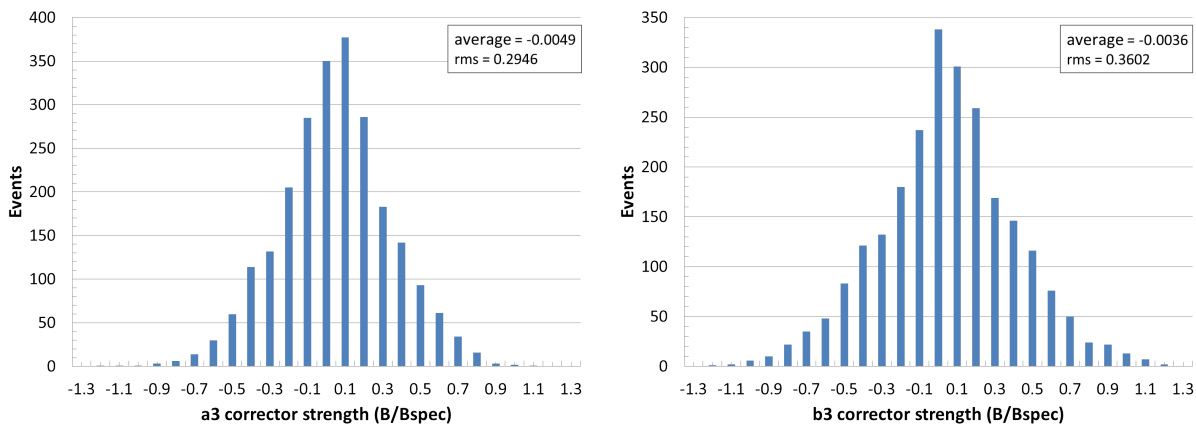

Fig. 28: Normalized strengths of the IT a_3 and b_3 correctors in 600 seeds for the round collision optics, where $a_{3\mathrm{U,R}} = 2$ and $b_{3\mathrm{U,R}} = 3$ in the IT quadrupoles and the D1 a_3 and b_3 errors are included.

7 Detailed baseline DA investigations for both beams

7.1 Impact of MCBXF field errors

The MCBXF magnets have two main functions, namely the generation of the orbit bumps for the parallel separation and the crossing schemes and the correction of the IT transverse misalignments. This

implies that the actual strength will be different for each magnet, as the former contribution is purely deterministic while the latter is variable and depends on the actual misalignment of each magnet. Hence, the magnetic field errors used in DA simulations have to be specified as absolute errors, and not relative to the main field strength, otherwise the impact of the FQ of these magnets might be severely underestimated. There are two classes of magnets, the MCBXFA magnets located in the non-linear corrector package, and the MCBXFB magnets located close to the Q2. Furthermore, there are magnets for the horizontal and the vertical plane, bringing the total to 24 magnets for IR1 and 5.

A first interesting aspect to investigate is whether the magnetic field errors of the MCBXF magnets could be corrected by means of the non-linear corrector package. To this end, the systematic b_3 and a_3 errors, which are the largest ones for the current design, have been varied to investigate the effect on the normal and skew sextupole corrector strengths. The results are shown in Fig. 29. As we see, there is indeed enough margin in the corrector strengths to use them to compensate for the MCBXF field errors. Of course, while these findings open the option to assume that the non-linear correctors are used to mitigate the potential field quality issues of the MCBXF, in practice, one should be more careful. In fact, one should ensure the capability of using the non-linear correctors since the beginning of the beam commissioning of HL-LHC and to manage also the dynamic variation of the MCBXF settings during the whole HL-LHC operational cycle. All this looks rather unrealistic, in particular in light of what occurred to the LHC, where the low-order non-linear correctors have been put in operation after about 10 years since the first circulating beams in the rings.

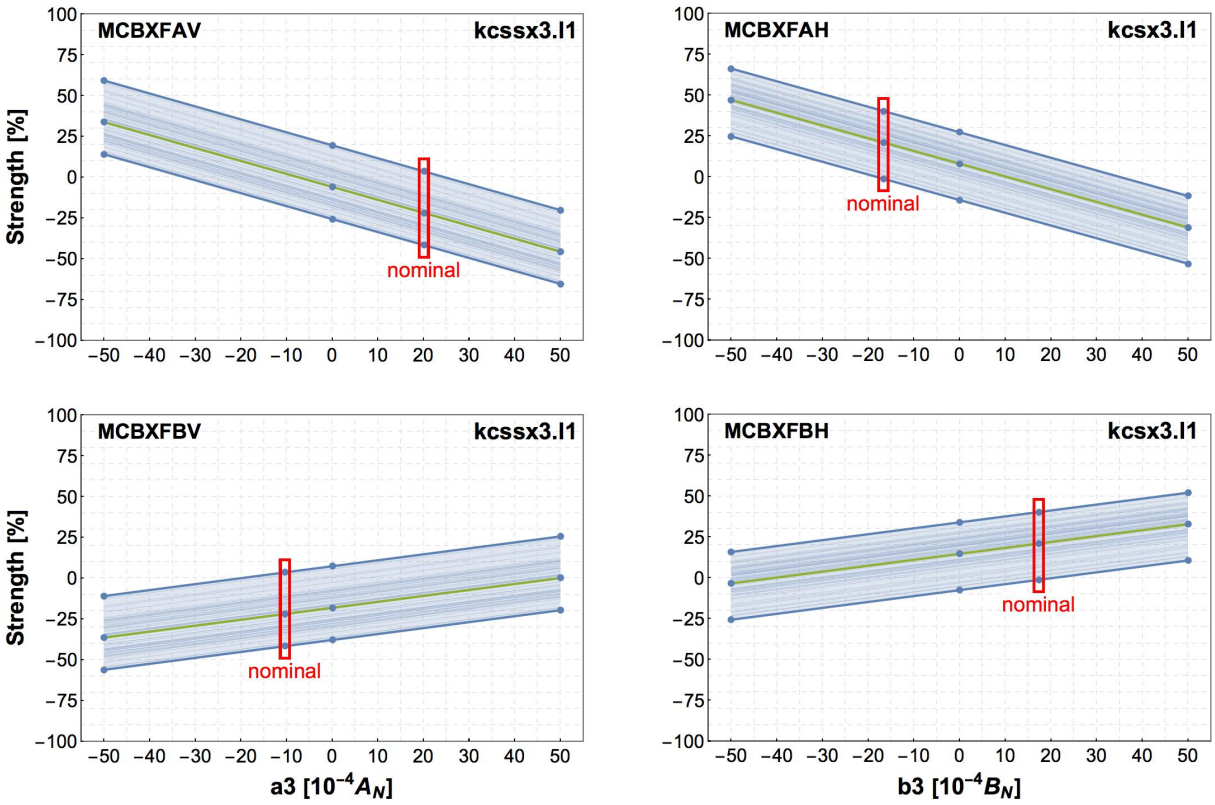

Fig. 29: Impact on the relative sextupole (normal and skew) corrector strength as a function of b_3 and a_3 errors of MCBXF for 60 seeds.

For these reasons, the impact on DA has been assessed by means of numerical simulations performed for several different scenarios. Contrary to the nominal set-up, 59 angles in the $x - y$ plane have been used for this simulation campaign and the results are shown in Fig. 30. In this type of plots one can recognise three thick lines, corresponding to $\mathrm{DA}_{\mathrm{min}}$, i.e. the minimum over angles and seeds, $\mathrm{DA}_{\mathrm{ave}}$,

i.e. the average over seeds and angles, and DA_{max}, i.e. the maximum over angle and seeds. The thinner lines represent the DA value averaged over the angles for the sixty seeds. Firstly, we notice that adding the nominal errors to the MCBXF magnets without the corresponding correction generates a clear drop of DA, as it decreases for all seeds, with the minimum DA being reduced by about $1\,\sigma$ and the average by about $0.5\,\sigma$. In case the sextupolar (normal and skew) errors are corrected, then the DA reaches its nominal level again. Furthermore, we performed a simulation where all MCBXF errors were assigned except for the b_3 and a_3 components. This is shown in Fig. 30 with the label MCBXF (HO), where HO stands for Higher Orders only. It is clear that there is almost no effect on the nominal DA, thus showing that the dominant MCBXF field errors are indeed b_3 and a_3. Lastly, we investigated whether one of the two classes (MCXBFA or MCBXFB) is dominant over the other, and indeed, the impact on the DA is clearly stronger for the MCBXFA magnets.

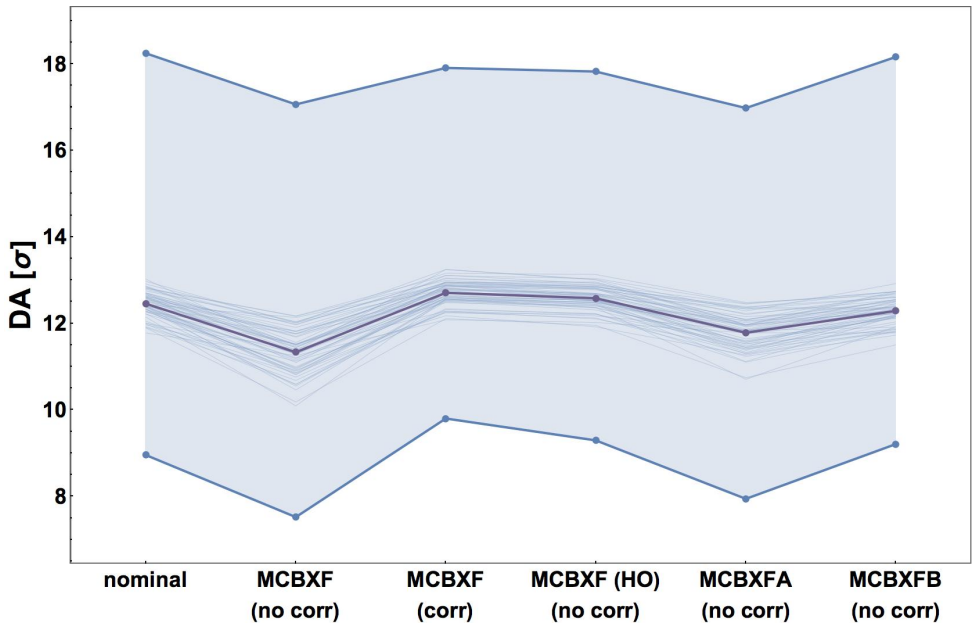

Fig. 30: Impact on DA of several scenarios referring to MCBXF errors.

7.2 Impact of triplet fringe fields and of magnet's families

In the first of these two small studies, we investigated the impact on DA of moving towards a more realistic simulation set-up. This is a set-up where we use expected instead of specified errors. It is worth reminding that while the former are produced by means of electromagnetic simulations, the latter have been produced by using the DA as a criterion to set bounds to each multipole and are the outcome of massive numerical simulations. In addition, a new approach had been implemented, namely based on the separation of the effect of the body of the triplet quadrupoles from that of the ends (see also Section 2). The results are shown in Fig. 31 (upper). We can clearly see that including expected error tables and fringe fields lowers the DA significantly, by about $0.5\,\sigma$ for the minimum and $2\,\sigma$ for the average, the final reduction is generated by the MCBXF field quality. Implicitly, this proves the efficiency of the optimisation performed when turning the expected errors into specified ones.

In the second study we added the errors for the new HL-LHC magnets step-by-step, starting from the arcs and then moving towards the IPs. The result is shown in Fig. 31 (lower). The impact on DA is of course very strong, as expected. The biggest jump occurs when adding errors of the D2 separation magnet, and then when the errors for the inner triplet quadrupoles are included, too. The former induces a loss of about $8\,\sigma$ in minimum DA and $5\,\sigma$ in average DA, while the latter induces a loss of about $2\,\sigma$ in minimum DA and $6\,\sigma$ in average DA. It is also worth noting that while the DA for the LHC (configuration

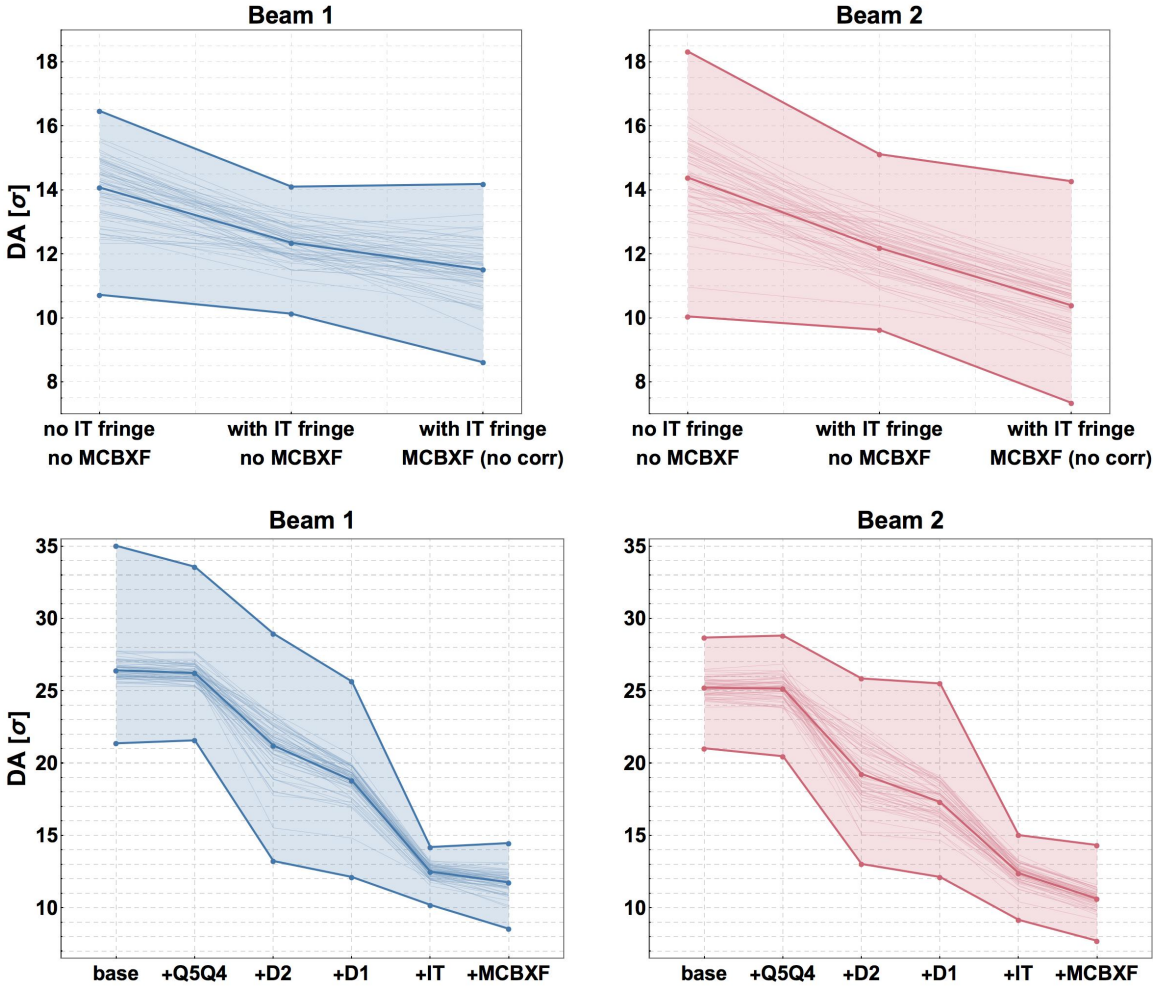

Fig. 31: Upper: Impact on DA of IT quadrupoles fringe-field effects. Lower: Impact on DA of the stepwise addition of HL-LHC magnets field quality, starting from the LHC baseline.

labelled as "base" in the plot) is strongly asymmetric between Beam 1 and 2, in particular in terms of the maximum DA (possibly due to the impact of outliers), the opposite occurs for the nominal HL-LHC configuration, where the maximum DA for Beam 2 is larger than that for Beam 1. It is clear that this approach does not allow drawing any conclusion about the relative impact of each magnet family, i.e. it is not possible to state that the D2 field quality has a stronger impact on DA than the triplet quadrupoles. This type of assessment would have required to include only a single magnet class for each DA simulation.

7.3 Impact of tune, chromaticity, and octupoles at injection

In this last study, we investigate the operational set-up at injection (see also Section 5). Firstly, we investigate the effect on DA of the chromaticity and octupole settings. This is shown in Fig. 32 showing the minimum (upper) and average (lower) DA. While the effect of chromaticity is rather strong, inducing a DA drop of about $2\,\sigma$ when going from 0 to $+20$ units, the effect of the octupoles is even stronger, with the DA going from $12\,\sigma$ in the minimum DA ($14\,\sigma$ in the average DA) at 0 A towards $4\,\sigma$ ($5.5\,\sigma$ in the average DA) at -40 A. Even though this effect is also present for positive octupole strength (at $+40$ A), the positive current is slightly better as far as DA is concerned, as it recovers about $1\,\sigma$ on both the minimum and the average DA.

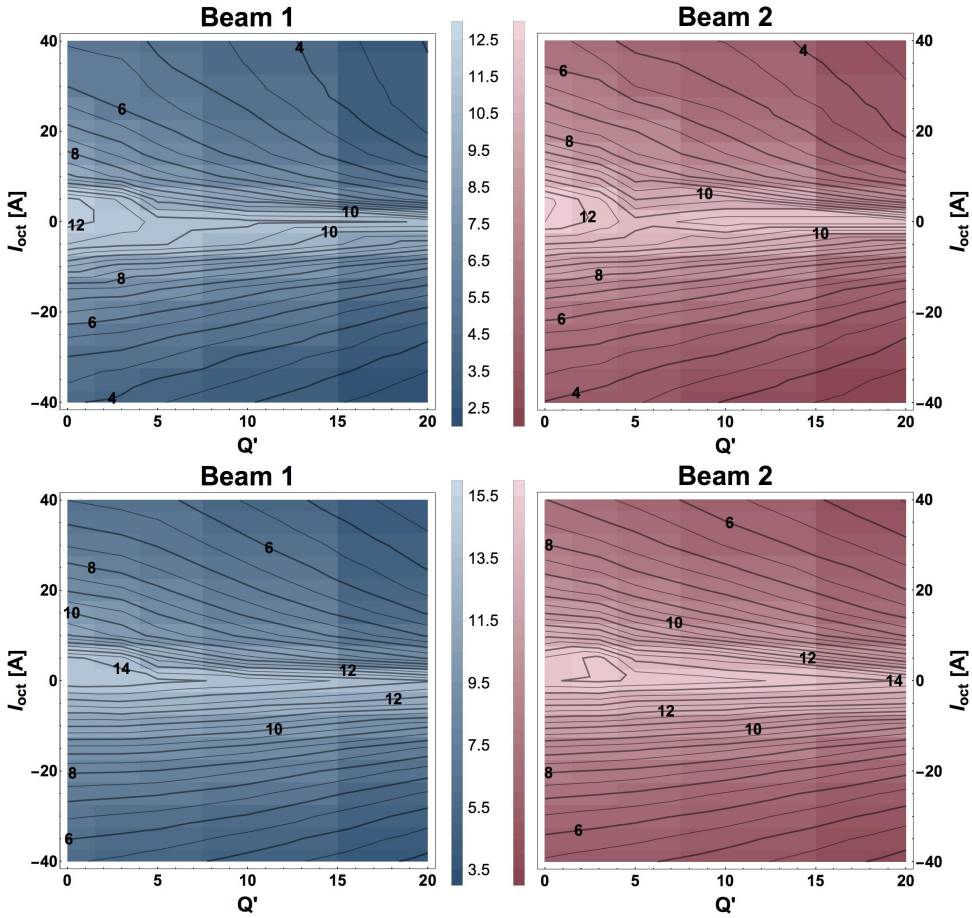

Fig. 32: Scan over octupoles and chromaticity at injection, showing minimum (upper) and average (lower) DA.

Secondly, we investigate whether the working point could be optimised. For this, we performed a tune scan around the current working point with worst-case chromaticity and octupole settings, as shown in Fig. 33, where the corresponding minimum (upper) and average (lower) DA are plotted. From this we can conclude that moving the working point towards $(62.27, 60.28)$ would imply a gain of about $2\,\sigma$ on the minimum and $1.5\,\sigma$ on the average DA. However care needs to be taken, as this investigation has been done without beam-beam effects and also without electron cloud effects, which have both a strong impact on the tune optimization process.

8 Detailed analysis of the performance of IT non-linear correctors

The HL-LHC design includes eight non-linear field correctors for each side of the interaction points in IR1 and 5 in order to compensate the normal and skew non-linear field components from $n = 3$ to $n = 6$ of the IT and D1 magnets. The correction of the IT non-linear field errors in SixTrack simulations is performed by setting the correctors strength to cancel certain high-order resonance driving terms based on analytical calculation and the known assigned IT errors [4]. The latter information may not be accurately known in the real machine (see, e.g. [20, 21] for an overview on the topic). Moreover, the procedure for the correctors set-up in operation may be different. Furthermore, the correctors strength may not be precisely known due to unavoidable uncertainty in the correctors transfer function. As a result, the operational IT correctors strength might differ from the ideal set-up used in the simulations. Furthermore, mechanical imperfections might affect the transverse position of the various corrector magnets or their roll angle. It is therefore important to evaluate how large is the impact of these effects on the DA.

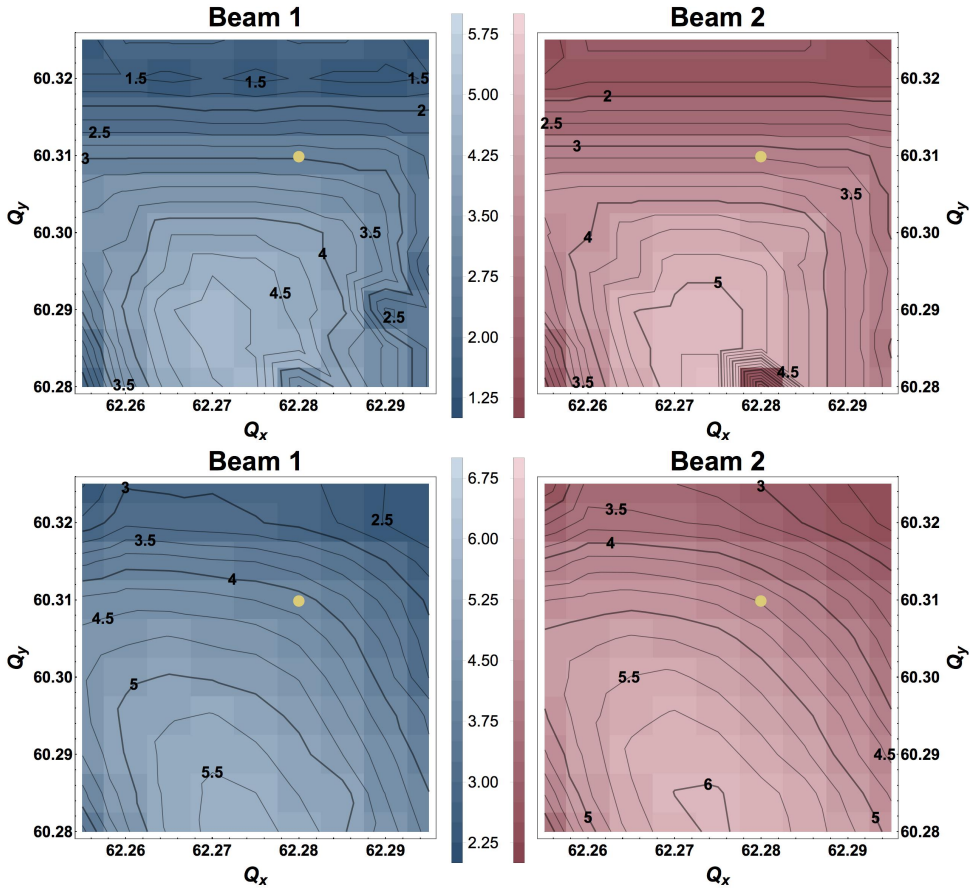

Fig. 33: Tune scan at injection with $I_{\text{oct}} = +40$ A, $Q' = 20$, showing minimum (upper) and average (lower) DA. The yellow dot is the baseline working point.

First of all, we would like to point out that the use of the IT non-linear field correctors is required only during the beta squeeze and collision in IP1/5, where β^* is low and the IT beta functions are very high, which strongly amplify the effects of the IT errors. To confirm this statement, Fig. 34 presents the DA of round collision optics at higher β^* during the pre-squeeze, where the IT correctors are turned on and off. It shows little difference between the two cases, thus confirming that the IT correctors are not necessary outside of the beta squeeze stage.

A very interesting study is to investigate how the DA depends on the presence of the non-linear corrector package. This is a very relevant point, as at the beginning of HL-LHC operation it will be hard to have mastered well enough the non-linear correctors to allow their full operational use. Therefore, the first investigation consists of switching correctors off on an order-by-order basis, as shown in Fig. 35, where the round collision optics has been selected, Landau octupoles are switched off and Q' is set to 3 units. The main feature to notice is that, overall, the effect is not dramatic on the average DA, with a maximum drop of about $0.5\,\sigma$, whilst the effect on the minimum DA is larger, with a drop of about $2\,\sigma$ when switching off the b_3/a_3 correctors. It is worth noting that the chromaticity is always corrected after having defined the setting of the non-linear correctors. Hence, the observed DA reduction in the case of b_3/a_3 correctors is not due to uncorrected chromaticity.

It is also worth observing that such a DA reduction is a consequence of the fact that on a seed-by-seed basis the DA variations are very strong, which is evidenced by the individual seed lines in Fig. 35 that can jump by several σ down, but also up, when switching off one corrector. The observed large DA increase is a sign that internal compensations occur and this is a warning sign that the result might strongly depend on the detail of actual errors in the various insertion magnets. A larger impact on

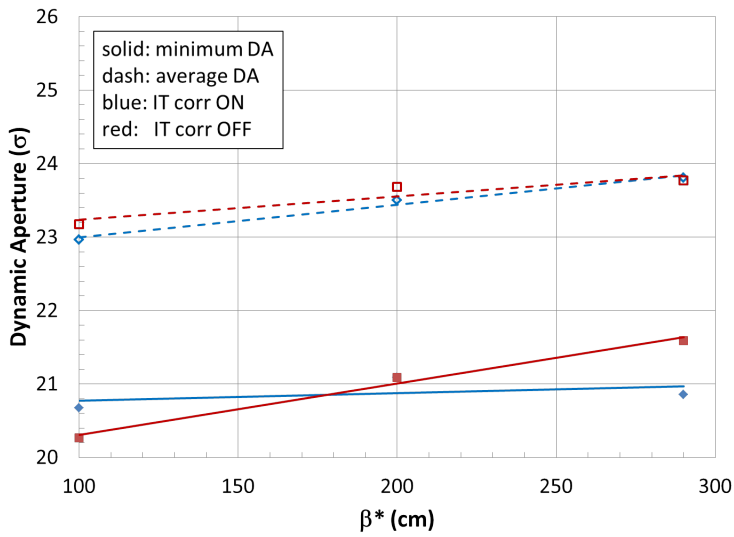

Fig. 34: DA of round collision optics vs β^* with the Landau octupoles set to the nominal strength of -570 A for two configurations of the IT non-linear field correctors, namely turned off and on.

Beam 2 DA with respect to Beam 1 is also observed, as well as stronger sensitivity to the status of b_4 and b_6 non-linear correctors.

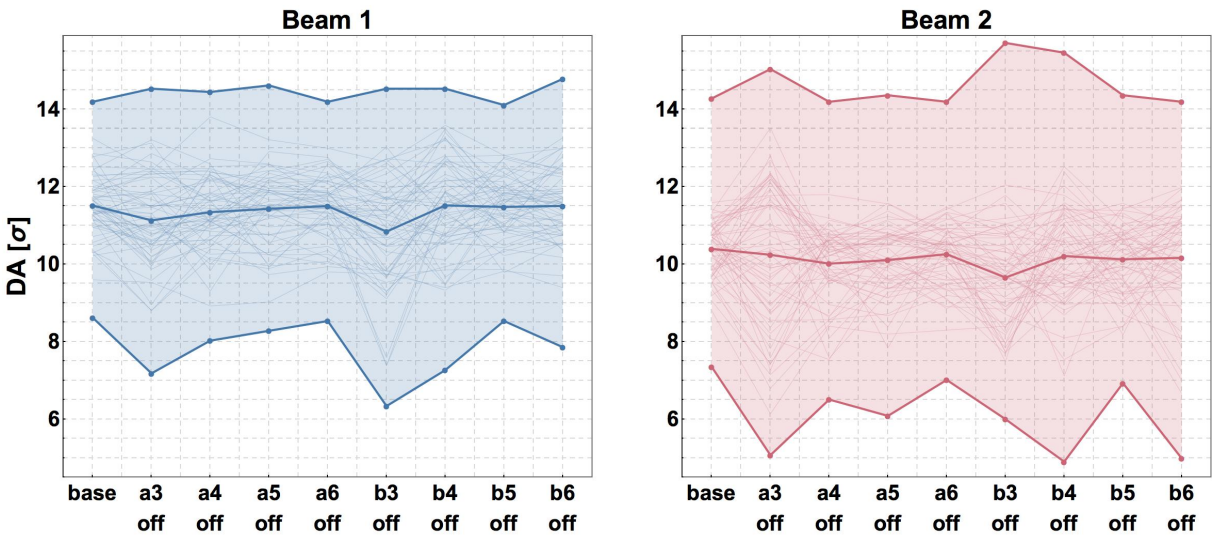

Fig. 35: Impact on DA of switching non-linear correctors off, order-by-order.

The next investigations look at two relevant configurations, namely a first one where only the new HL-LHC correctors are switched off, i.e. the a_5, b_5, and a_6 correctors that are not present in the LHC layout, and a second one where all correctors are switched off, to mimic the situation at the beginning of HL-LHC operation. The DA results are shown in Fig. 36 and as it can be expected, the impact on DA accumulates, and in the worst-case scenario where all correctors are switched off we lose about $3\,\sigma$ on the minimum and a bit more than $1.5\,\sigma$ on the average DA and for Beam 2 the situation is worse, thus confirming a stronger sensitivity of the DA on the magnetic errors. Overall the individual seed lines are highly scattered, confirming once more the presence of internal compensations.

In the next set of studies, performed with expected error tables, we want to test the robustness of

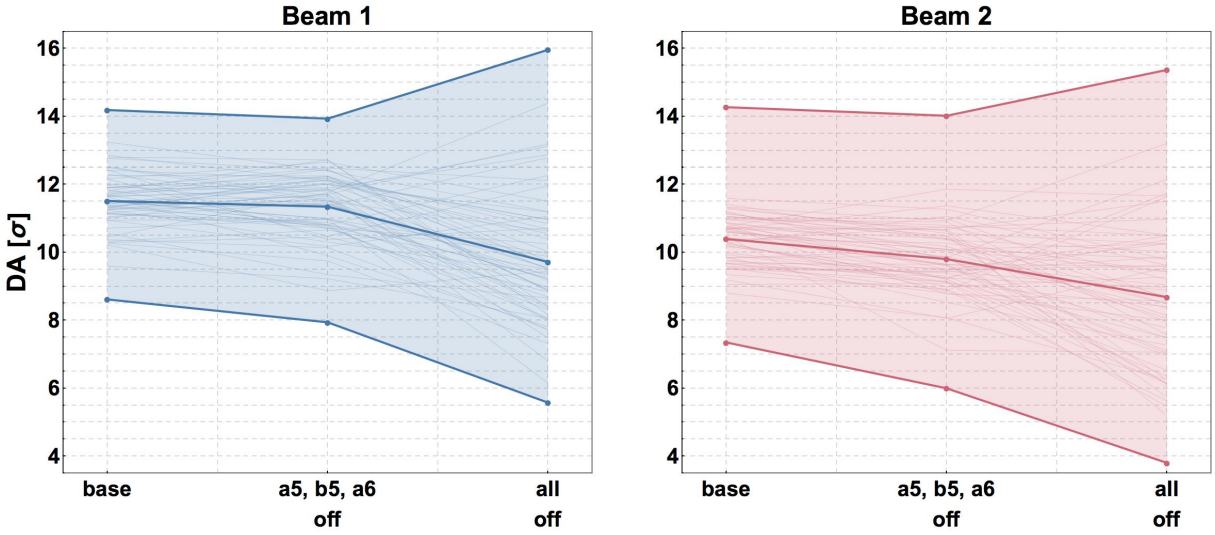

Fig. 36: Impact on DA of switching non-linear correctors off, for the cases where only the a_5, b_5, a_6 correctors are off, and where all are off.

the performance of the non-linear correctors under mispowering or mechanical misalignments. We use the term mispowering to indicate that the corrector strength computed by the standard algorithm, based on resonant driving term minimization, is changed prior to being applied to the configuration for the DA simulation. In this way, we simulate several effects, namely the inaccuracy with which the transfer function of the correctors is known, or, equally, the inaccuracy with which the field quality of the triplet quadrupoles or D1 separation dipoles is known, or the impact from beta-beating that is absent in our simulations given that only multipoles of order $n \geq 3$ are included in the SixTrack simulations. The assumed order of magnitude of the mispowering effects is such to represent the impact of the combination of the three effects mentioned above. A series of configurations in which these effects are applied on an order-by-order basis have been carried out. Then the combined effect is probed by generating 64 random mispowering or misalignment realisations, out of the huge set of possible realisations of these effects, for all correctors simultaneously. Moreover, all configurations come in two variants, namely one with and one without correction of D2 (see also Section 9): although we will present only the results corresponding to the standard approach for the use of the no-linear correctors, i.e. not including the correction of the field quality of the D2, the results and the trends are essentially the same as those presented here.

Firstly, we start by probing the impact of mispowering. To this end, we assume that any mispowering comes from a scaling of the β-function, hence the magnitude of the mispowering depends on the order of the corrector. Estimating a possible error in the value of the β function of $\pm 10\%$, the mispowerings scale from $\pm 15\%$ for $n = 3$ order to $\pm 30\%$ for $n = 6$ and the corresponding results of these simulations are shown in Fig. 37. The upper figure shows the DA when mispowering the normal correctors, while the lower one shows the DA when mispowering the skew correctors. We see that the overall effect is quite small, both when looking at the minimum and the average DA. The results shown are for the case where the D2 errors are not corrected. When including D2 correction, the DA is of course increased as the algorithm is quite efficient (see also Section 9), but more importantly the same flat behaviour is observed, with two small exceptions where a trend is visible: the b_3 correctors show some linear impact on DA in Beam 1 (clear, but not large, as it is less than $1\,\sigma$ difference on the minimum and less than $0.5\,\sigma$ difference on the average), but this is not present in Beam 2. Moreover, there is a clear dependence in the minimum DA on the b_6 correctors in Beam 2 (quite pronounced with $1\,\sigma$ difference), but this is not present in Beam 1 and more importantly it is barely visible in the average DA.

It is clear that the expected range of mispowerings on the correctors has no drastic impact on their

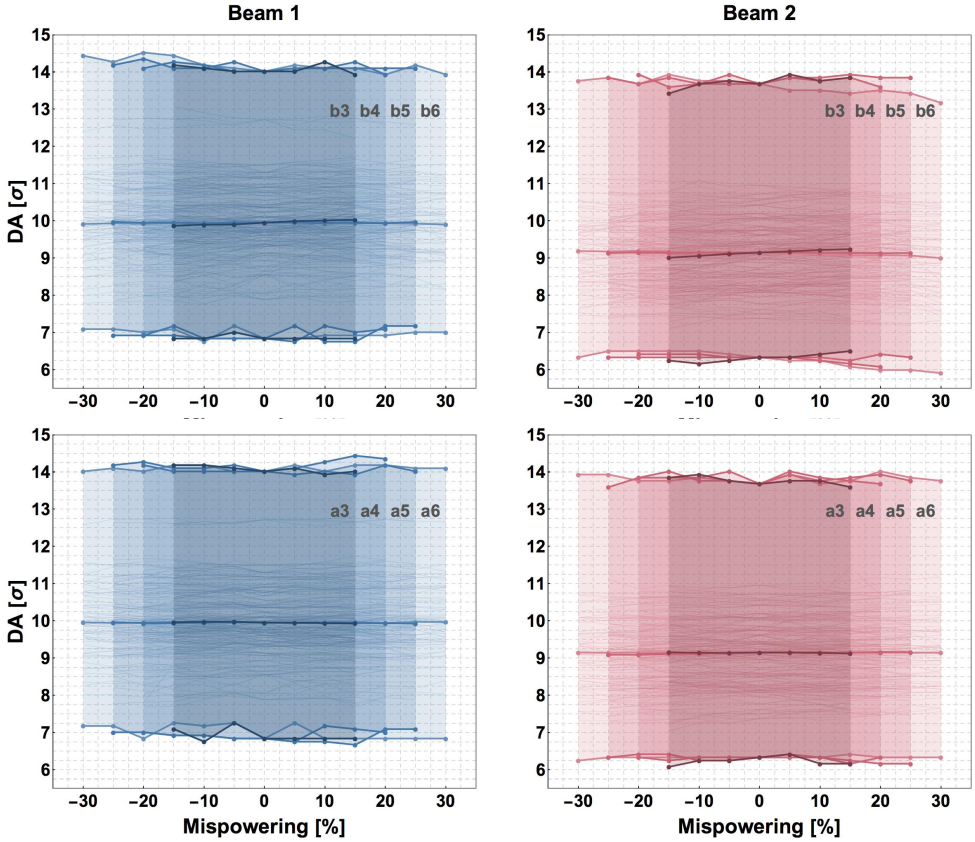

Fig. 37: Mispowering of normal (upper) and skew (lower) correctors, without correction of D2 field quality. Note that in these studies the latter is chosen to be a worst-case scenario, i.e. $b_3 = 3.8$.

performance, at least not when mispowering step-by-step and order-by-order. To complete this study, we performed an investigation over 64 random realisations, where every individual corrector is assigned a different mispowering (uniformly sampled). This is to mimic possible real-life scenarios and investigate how the non-linear correctors would perform in this case, in view of assessing the presence of strong interplay between them. Figure 38 shows a histogram per beam of the average DA of each realisation, for the case without D2 correction. The effect is clearly very small. In both cases the average of the distribution shifts not more than $0.05\,\sigma$ from the reference value, while the distribution remains sharply peaked with a maximum standard deviation of $0.07\,\sigma$. The case with D2 correction showed, except for an overall increase of the DA, exactly the same behaviour. Hence, we can safely conclude that the current system of non-linear correctors is robust under the expected types of mispowerings.

In a second study we investigate the effect of possible misalignments. This study is much more involved than the former one, as the effect can manifest as an x-, y-, or ψ-misalignment (rotation around the s-axis, i.e. a roll angle error), tripling the amount of simulations. We take a safe margin and scan misalignments up to ± 1 mm and ± 1 mrad, which is the worst-case lower limit of our current placement accuracy, always using a uniform distribution for the misalignments. The results of the order-by-order analysis, where all correctors of the same order are misaligned by the same amount, are shown in Fig. 39 for misalignments in the x-direction. The situation is very similar to the mispowering investigation. No trends are visible and fluctuations are never bigger than $0.5\,\sigma$. The average DA even shows an almost perfectly flat behaviour (any dependencies that arise have a maximum impact of $0.1\,\sigma$). Very similar results have been observed for misalignments in the y-direction as well as for misrotations.

The expected range of correctors misalignments has no drastic effect on their performance, at least not for step-by-step and order-by-order scenarios. To complete this study, we performed an investigation

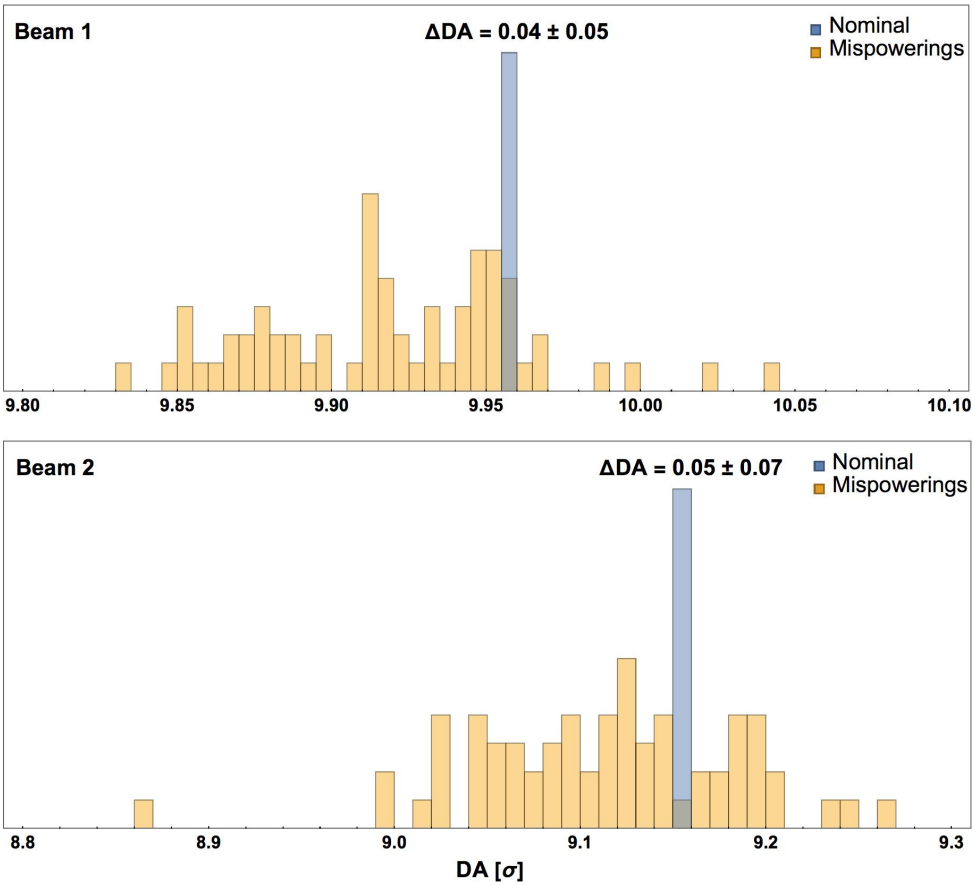

Fig. 38: Histogram of DA for 64 random mispowering realisations, without correction of D2 field quality.

similar to that carried out for the case of mispowerings, i.e. scanning over 64 random misalignment realisations, where every individual corrector is assigned a different misalignment, uniformly sampled. This is again to mimic possible real-life scenarios and investigate how the non-linear correctors would perform in this case. However, to limit the number of performed simulations, we only investigated the case where D2 is corrected. Figure 40 shows a histogram per beam of the average DA of each realisation. The effect is, as before, clearly very small. In all cases the peak of the distribution shifts not more than $0.02\,\sigma$ from the nominal value, while the distribution remains sharply peaked with a maximum standard deviation of $0.06\,\sigma$.

We can hence safely conclude that the current system of non-linear correctors is rather robust under all expected types of mispowerings and misalignments. Mispowering and/or misaligning the correctors order-by-order does not show any significant impact on DA, and when applying a randomised set of mispowerings or misalignments, there is virtually no shift in average DA nor is there a clear spreading of its distribution.

9 Correction of D1 and D2 field quality with IT non-linear correctors

Following the results of the previous section, we see that the errors in D2 have a strong impact on the DA and we study if part of the reduction in DA can be recovered by correcting the errors in D2 with the non-linear correction package [22]. This is however not trivial, as D2 has two apertures while the non-linear correctors have only one. Hence both beams need to be compensated simultaneously by using the average of the magnetic errors of both D2 apertures. The systematic errors in D2 are antisymmetric for even and symmetric for odd orders, while the skew components have no systematic part. In other words, only b_3 and b_5 can be corrected. Indeed, all multipolar errors up to $n = 6$ could be corrected for

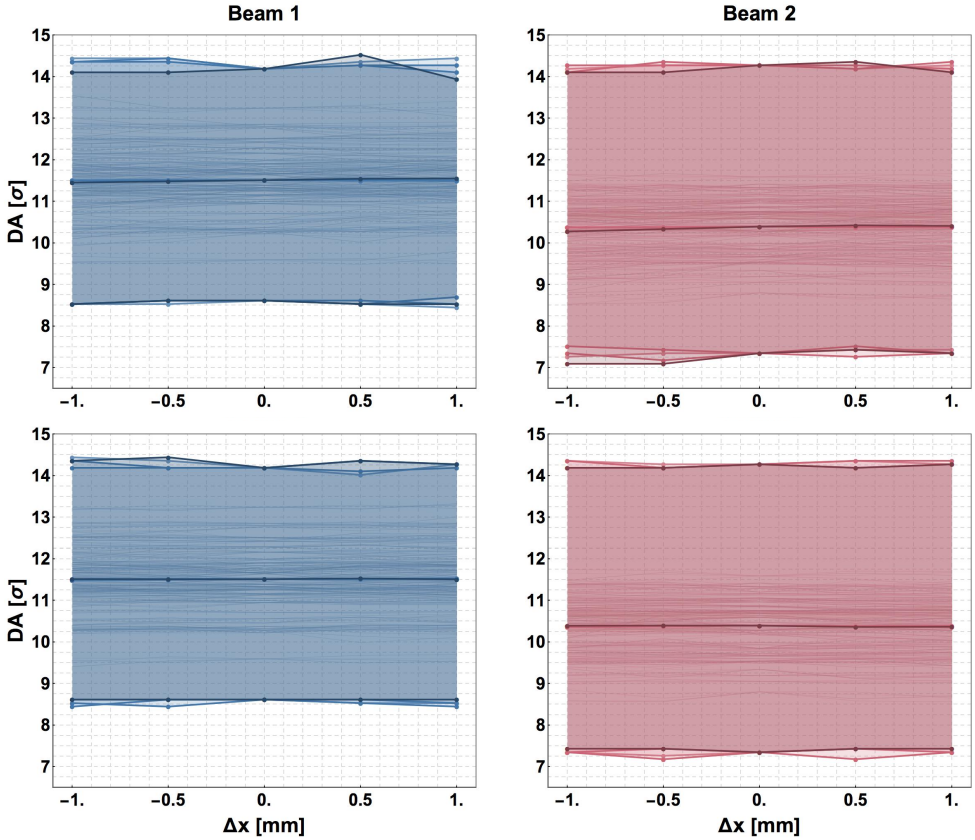

Fig. 39: Misalignment in x-direction of normal (upper) and skew (lower) correctors, without correction of D2 field quality.

the average component between the two apertures. However, it is clear that such an average would be small, except for the systematic multipoles. Hence, this is not worth the effort of devising a dedicated compensation approach and we will focus on the systematic b_3 corrections, although attempts to correct also b_5 where made without much success.

As a first test, we probed the efficiency of the correction algorithm in compensating for the field quality of the D1 separation dipole. We scanned over different values of the b_3 systematic component for this magnet with and without the correction algorithm. The results are shown in Fig. 41 (upper), where it is apparent that when allowing the D1 errors to be corrected, the DA remains constant over a wide range of values of the systematic b_3 error. Also shown is the nominal value of b_3 (-0.9 units) for which we conclude that the correction algorithm gains back a bit more than $1\,\sigma$ on the minimum DA and $0.5\,\sigma$ on the average DA for Beam 1 (and similar values, though not as pronounced, for Beam 2). The gain is even larger for larger $b_{3\mathrm{S}}$ values.

This study can be repeated for the D2 errors, as shown in Fig. 41 (lower). Also in this case the correction algorithm manages to recover the DA when varying the systematic b_3 component of D2, even though there is a very mild downward trend for the DA after correction for positive $b_{3\mathrm{S}}$ values. At the nominal value for b_3 (1 unit), the correction algorithm recovers about $0.5\,\sigma$ in both the minimum and average DA for Beam 1 (and, as was the case for D1, a bit less for Beam 2). However, larger values for $b_{3\mathrm{S}}$ might be expected, up to values of 3.8 units [15]. In that case, as also shown in Fig. 41, correcting D2 regains at least $2\,\sigma$ for both the minimum and average DA for Beam 1 (and again a bit less for Beam 2). It is in this case that the new correction approach becomes indispensable. Clearly, the successful test of this new approach should be cross-checked against the increased need for strength of the sextupolar corrector. The outcome of these investigations is shown in Fig. 42. There is clearly enough margin to

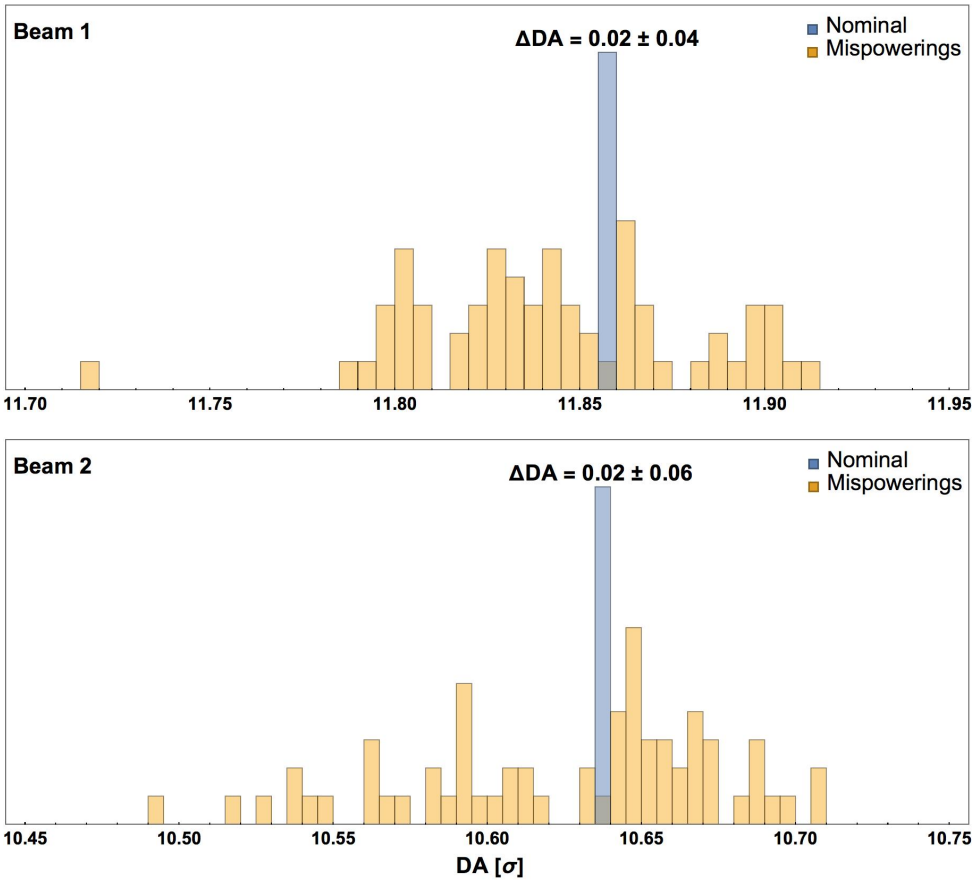

Fig. 40: Histogram of DA for 64 random misalignments realisations, with correction of D2 field quality.

add the field quality of D2 to the correction algorithm, as even in the worst case (where the systematic b_3 of D2 has a value of 3.8 units), only an increase of about 10% in strength is needed. This would bring the total strength, i.e. what is needed to cope with the IT, D1, and D2 FQ, at about $\pm 30\%$ at most, thus leaving enough operational margin.

Finally, it is worth mentioning that we started adapting the correction algorithm to allow for the correction of the systematic b_5 error of D2. However, while the algorithm works as expected when scanning over the systematic b_5 of D1, it does not succeed in recovering the nominal DA in the case of D2. This study is still in progress.

10 Conclusions

This report gathers together the results of several tracking campaigns carried out to study the detailed performance of the HL-LHC V1.0 optics and layout in terms of dynamic aperture without beam-beam effects. These CPU-intensive simulation campaigns cover a time interval of few years, which explains the lag between these results and the fact that the current nominal optics and layout version is 1.4. In all future simulation campaigns the operational values of the linear chromaticity and of the octupoles will be used. Moreover, as it was started in these studies, the expected values of the magnetic multipoles or the values obtained by magnetic measurements will be used, instead of those obtained by optimising the DA value as it was done in the past.

Thanks to these simulations a rather clear picture about the sensitivity of the dynamic aperture as a function of several machine parameters, such as tune, chromaticity, octupole strength, as well as the field quality of individual magnets classes has been depicted. Among the several studies presented, it is

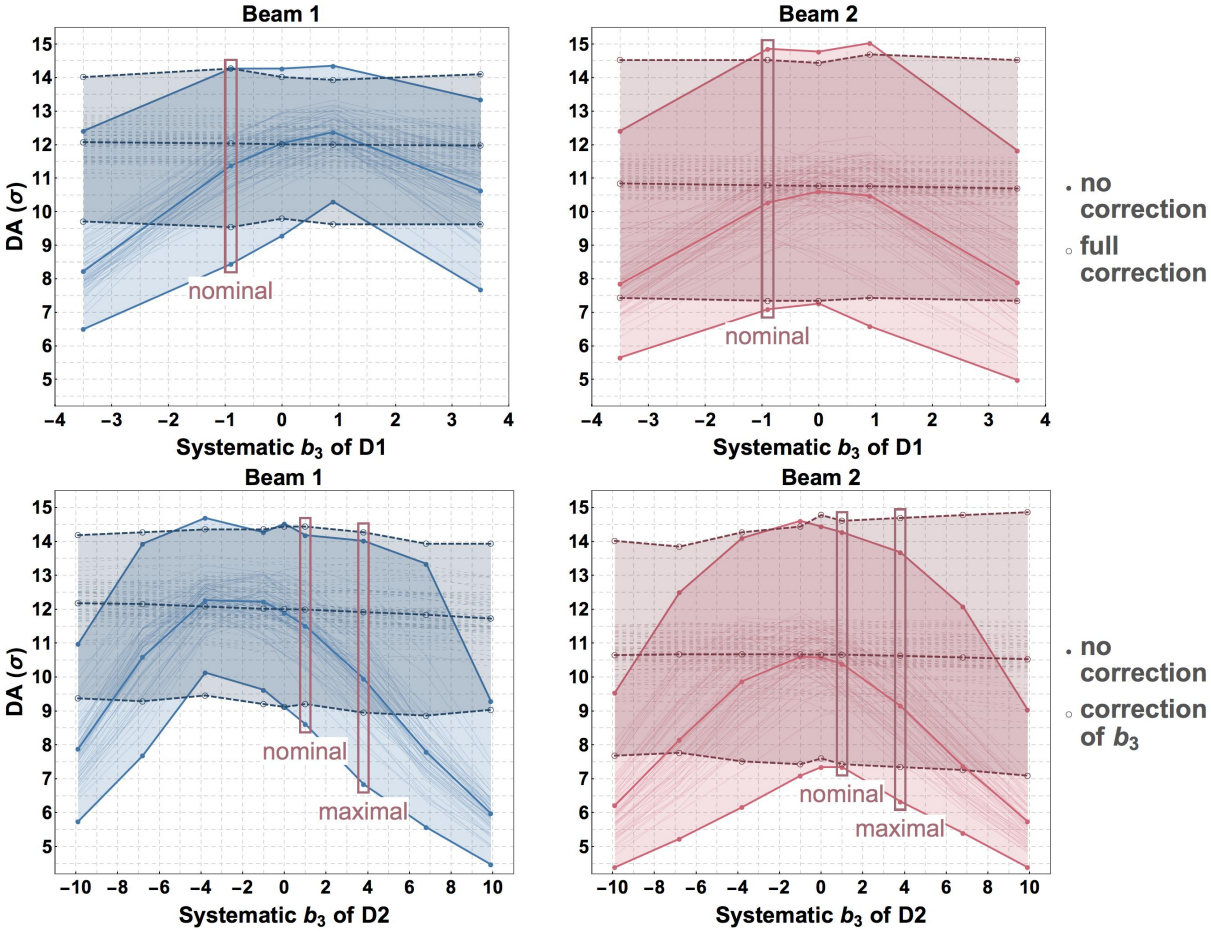

Fig. 41: Dynamic aperture as a function of b_3 systematic component of D1 (upper) and D2 (lower) for both beams with and without compensation by means of the non-linear correctors.

worthwhile mentioning that the study on the impact of mispowering and misalignment of the non-linear correctors has provided a very useful input to the definition of the mechanical tolerances and also on the accuracy of the correction strategy.

It is particularly important to stress that the recent results about the impact of the larger-then-expected measured multipolar errors of the triplet quadrupoles led to the decision of increase the length on the corrector magnets from $n = 3$ to $n = 5$ in order to increase their strength so to mitigate possible further increase of the corresponding multipoles. In addition, the length of the skew quadrupole corrector has been reduced so to keep the overall length of the corrector package unchanged. All these changes have been incorporated into the new HL-LHC V1.4.

Among the next steps for these type of studies we would like to highlight the moving to the latest optics layout 1.4, where the key change is the fact that the Q4 and Q5 magnets will be the corresponding existing LHC magnets, thus requiring a change in the strategy of the magnetic error assignment. Therefore, starting from this layout version, the only statistical assignment of magnetic field error will be for the triplet quadrupoles and the D1 and D2 separation dipoles (and possibly the crab cavities). A small reduction of the dynamic aperture is also to be expected, due to an increase of about 4% of the peak β-function in the triplet for the same β^*, due to change in the triplet layout introduced in version 1.2. Also, the 11 T dipoles will be always included in the future DA simulations.

Finally, the next studies will also scrutinise the recent results concerning the measured field quality of the D2 separation dipole and the MCBRD orbit correctors [23].

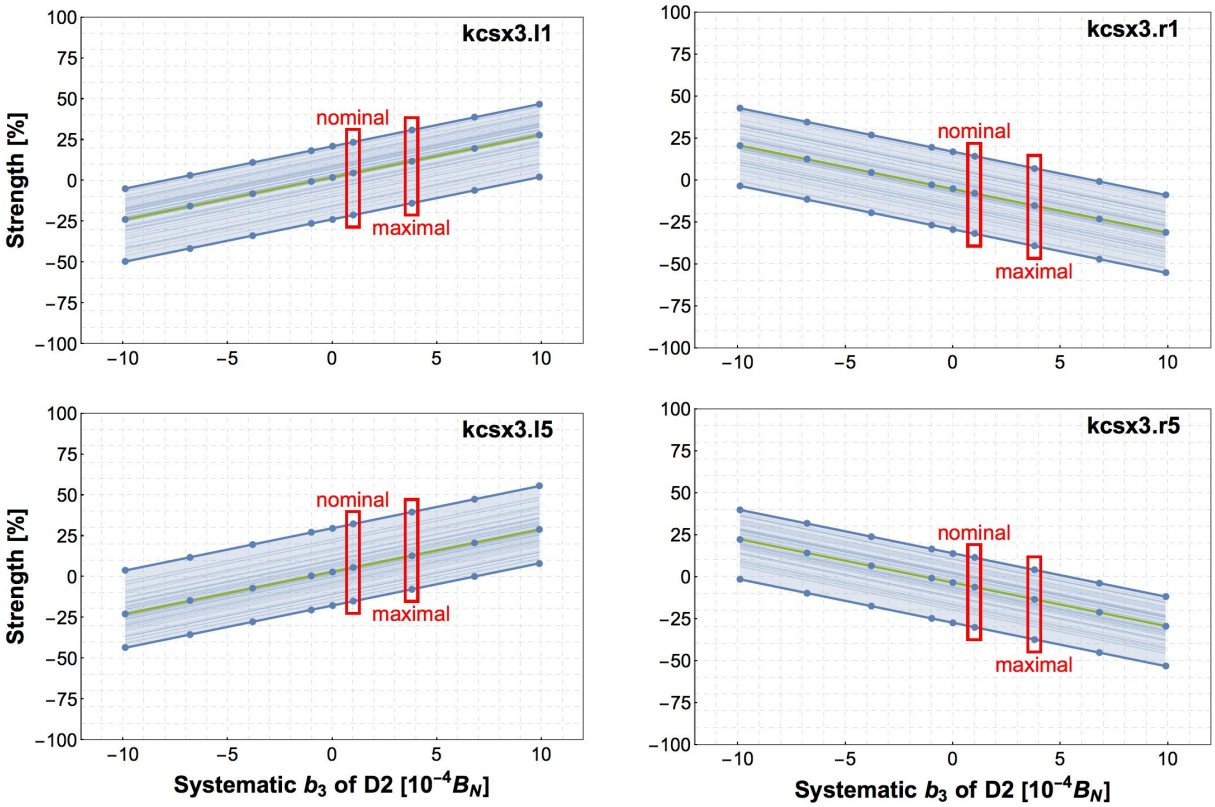

Fig. 42: Impact on sextupole relative corrector strength as a function of the b_3 systematic component of D2 for a set of 60 seeds.

Acknowledgements

We would like to thank S. Fartoukh for the tools developed for carrying out DA simulations. The constant help and support of A. Mereghetti for the BOINC submission has been essential for the successful completion of these studies. G. Arduini is warmly thanked for useful discussions, support and excellent comments on the original version of the manuscript. E. Todesco is also acknowledged for discussions and support. The comments of O. Brüning and L. Rossi on the final version of the manuscript are also warmly acknowledged.

This research has been supported by the HL-LHC project. Part of this research is supported by the U.S. DOE via the US-LARP program and the DOE Contract DE-AC02-76SF00515.

The LHC@home volunteers are warmly thanked as their CPU-time contribution was essential for the massive tracking campaigns carried out in the framework of the studies described in this report.

References

[1] R. de Maria, S. Fartoukh, A. Bogomyagkov, M. Korostelev, "HLLHCV1.0: HL-LHC Layout and Optics Models for 150 mm Nb_3Sn Triplets and Local Crab-Cavities", IPAC'13, Shanghai, May 2013, p. 1358 (2013).

[2] F. Schmidt, "SixTrack - Version 4.2.16 - Single Particle Tracking Code Treating Transverse Motion with Synchrotron Oscillations in a Symplectic Manner - User Reference Manual", CERN/SL/94-56 (AP) update (2012).

[3] `http://sixtrack-ng.web.cern.ch/sixtrack-ng/`

[4] M. Giovannozzi, S. Fartoukh, R. de Maria, "Specification of a System of Correctors for the Triplets and Separation Dipoles of the LHC Upgrade", IPAC'13, Shanghai, May 2013, p. 2612 (2013).

[5] D. Angal-Kalinin *et al.*, "Chapter 2: Machine Layout and Performance", Chapter 2 in High-Luminosity Large Hadron Collider (HL-LHC): Preliminary Design Report, arXiv:1705.09447, 10.5170/CERN-2015-005.21 (2015).

[6] High-Luminosity Large Hadron Collider (HL-LHC). Technical Design Report V.0.1, edited by G. Apollinari, I. Bejar Alonso, O. Brüning, P. Fessia, M. Lamont, L. Rossi, L. Tavian, CERN Yellow Reports: Monographs, Vol.4/2017, CERN-2017-007-M (CERN, Geneva, 2017). https://doi.org/10.23731/CYRM-2017-004.

[7] L. Fiscarelli, M. Giovannozzi, P.D. Hermes, S. Izquierdo Bermudez, S. Russenschuck, F. Savary,"Field Quality of MBH 11-T Dipoles for HL-LHC and Impact on Beam Dynamic Aperture", IEEE Trans. Appl. Supercond. **28** 4004005 (2018).

[8] B. Bellesia, J.-P. Koutchouk, E. Todesco, "Field Quality in Low-β Superconducting Quadrupoles and Impact on the Beam Dynamics for the Large Hadron Collider Upgrade", Phys. Rev. ST-AB **10**, 062401 (2007).

[9] `/afs/cern.ch/eng/lhc/optics/HLLHCV1.0/errors/`

[10] Y. Nosochkov, Y. Cai, M.-H. Wang, S. Fartoukh, M. Giovannozzi, R. De Maria, E. McIntosh, "Field Tolerances for the Triplet Quadrupoles of the LHC High Luminosity Lattice", IPAC'12, New Orleans, May 2012, p.169 (2012).

[11] Y. Nosochkov, Y. Cai, M.-H. Wang, S. Fartoukh, M. Giovannozzi, R. De Maria, E. McIntosh, "Optimization of Triplet Quadrupoles Field Quality for the LHC High Luminosity Lattice at Collision Energy", IPAC'13, Shanghai, May 2013, p. 1364 (2013).

[12] S. Fartoukh, private communication.

[13] S.I. Bermudez, "MQXFS Magnetic Measurements and Analysis", 6th HL-LHC Collaboration Meeting, Paris, November 14-16, 2016.

[14] E. Todesco,"Multipolar content of triplet magnets", HL-LHC WP2 meeting, February 28, 2017 `https://indico.cern.ch/event/614829/`

[15] E. Todesco, private communication.

[16] R. De Maria, S. Fartoukh, M. Giovannozzi, "Specifications of the Field Quality at Injection Energy of the New Magnets for the HL-LHC Upgrade Project", IPAC'13, Shanghai, May 2013, p. 2603 (2013).

[17] Y. Nosochkov, Y. Cai, M.-H. Wang, R. de Maria, S. Fartoukh, M. Giovannozzi, E. McIntosh, "Optimization of Triplet Quadrupoles Field Quality for the LHC High Luminosity Lattice at Collision Energy", IPAC'13, Shanghai, May 2013, p. 1364 (2013).

[18] Y. Nosochkov, Y. Cai, M.-H. Wang, S. Fartoukh, M. Giovannozzi, R. de Maria, E. McIntosh, "Specification of Field Quality in the Interaction Region Magnets of the High Luminosity LHC Based on Dynamic Aperture", IPAC'14, Dresden, June 2014, p. 1013 (2014).

[19] R. de Maria, M. Giovannozzi, E. McIntosh, Y. Cai, Y. Nosochkov, M-H. Wang, "Dynamic aperture studies for the LHC High Luminosity lattice", IPAC'15, Richmond, May 2015, p. 705 (2015).

[20] E. Maclean, *et al.*, "New Methods for Measurement of Nonlinear Errors in LHC Experimental IRs and Their Application in the HL-LHC", IPAC'17, Copenhagen, May 2017, p. 3155 (2017).

[21] F.C. Carlier, *et al.*, "Optics Measurements and Correction Challenges for the HL-LHC", CERN-ACC-2017-0088 (2017).

[22] M. Giovannozzi, S. Fartoukh, R. De Maria, "Initial models of correction systems", MILESTONE: M24.28 CERN-ACC-2014-0010 (2013).

[23] E. Todesco, "Progress on magnets for the HL-LHC insertion regions", talk at the HiLumi Annual meeting, CERN (2018).

Appendices

A Expected and optimised error tables

For the sake of reference some old expected error tables for the IT magnets and the corresponding optimised tables [11] are reported here.

Table A.1: Expected to achieve field errors in 150 mm aperture quadrupoles at $R_{\mathrm{ref}} = 50$ mm (error table "target6").

n	$a_{n,\mathrm{S}}$	$a_{n,\mathrm{U}}$	$a_{n,\mathrm{R}}$	$b_{n,\mathrm{S}}$	$b_{n,\mathrm{U}}$	$b_{n,\mathrm{R}}$
3	0	0.800	0.800	0	0.820	0.820
4	0	0.650	0.650	0	0.570	0.570
5	0	0.430	0.430	0	0.420	0.420
6	0	0.310	0.310	0.800	1.100	1.100
7	0	0.190	0.190	0	0.190	0.190
8	0	0.110	0.110	0	0.130	0.130
9	0	0.080	0.080	0	0.070	0.070
10	0	0.040	0.040	0.150	0.200	0.200
11	0	0.026	0.026	0	0.026	0.026
12	0	0.014	0.014	0	0.018	0.018
13	0	0.010	0.010	0	0.009	0.009
14	0	0.005	0.005	-0.040	0.023	0.023

Table A.2: Optimized error table "target65" at $R_{\mathrm{ref}} = 50$ mm.

n	$a_{n,\mathrm{S}}$	$a_{n,\mathrm{U}}$	$a_{n,\mathrm{R}}$	$b_{n,\mathrm{S}}$	$b_{n,\mathrm{U}}$	$b_{n,\mathrm{R}}$
3	0	0.800	0.800	0	0.820	0.820
4	0	0.650	0.650	0	0.570	0.570
5	0	0.086	0.086	0	0.084	0.084
6	0	0.155	0.062	0.800	0.550	0.550
7	0	0.152	0.095	0	0.095	0.095
8	0	0.088	0.055	0	0.065	0.065
9	0	0.064	0.040	0	0.035	0.035
10	0	0.040	0.032	0.075	0.100	0.100
11	0	0.026	0.0208	0	0.0208	0.0208
12	0	0.014	0.014	0	0.0144	0.0144
13	0	0.010	0.010	0	0.0072	0.0072
14	0	0.005	0.005	-0.020	0.0115	0.0115

B Selected error tables used in the tracking studies

For the sake of reference, the error tables for HL-LHC magnets used in the studies discussed in this report are listed in the following.

Table B.1: MCBXF expected error tables. Currently only systematic errors are assigned, as there are no estimates yet for the uncertainty and random components. There are two types of correctors: MCBXFA and MCBXFB, with different errors in the horizontal and vertical planes.

	7 TeV				450 GeV			
MCBXF:	A,H	A,V	B,H	B,V	A,H	A,V	B,H	B,V
$b2$	0	0	0	0	0	0	0	0
$b3$	-16.65	0	17.37	0	-16.65	0	17.37	0
$b4$	0	0	0	0	0	0	0	0
$b5$	-0.35	0	2.49	0	-0.35	0	2.49	0
$b6$	0	0	0	0	0	0	0	0
$b7$	0.98	0	0.62	0	0.98	0	0.62	0
$b8$	0	0	0	0	0	0	0	0
$b9$	0.07	0	-0.75	0	0.07	0	-0.75	0
$b10$	0	0	0	0	0	0	0	0
$b11$	4.3	0	3.6	0	4.3	0	3.6	0
$b12$	0	0	0	0	0	0	0	0
$b13$	0	0	0	0	0	0	0	0
$b14$	0	0	0	0	0	0	0	0
$b15$	0	0	0	0	0	0	0	0
$a2$	0	0	0	0	0	0	0	0
$a3$	0	20.12	0	-10.33	0	20.12	0	-10.33
$a4$	0	0	0	0	0	0	0	0
$a5$	0	-3.04	0	-3.6	0	-3.04	0	-3.6
$a6$	0	0	0	0	0	0	0	0
$a7$	0	-3.98	0	-3.26	0	-3.98	0	-3.26
$a8$	0	0	0	0	0	0	0	0
$a9$	0	-0.62	0	-0.58	0	-0.62	0	-0.58
$a10$	0	0	0	0	0	0	0	0
$a11$	0	0.02	0	0.12	0	0.02	0	0.12
$a12$	0	0	0	0	0	0	0	0
$a13$	0	0	0	0	0	0	0	0
$a14$	0	0	0	0	0	0	0	0
$a15$	0	0	0	0	0	0	0	0

Table B.2: IT FQ specification `IT_errortable_v66_5` at collision and injection energies, where the 7 TeV terms $b_{10\mathrm{S}}$, $b_{14\mathrm{S}}$, $b_{6\mathrm{U}}$ - $b_{14\mathrm{U}}$, $b_{6\mathrm{R}}$ - $b_{14\mathrm{R}}$, $a_{7\mathrm{U}}$ - $a_{9\mathrm{U}}$, and $a_{7\mathrm{R}}$ - $a_{11\mathrm{R}}$ are optimized.

	7 TeV			450 GeV		
	S	U	R	S	U	R
$b2$	0	0	10	0	0	10
$b3$	0	0.82	0.82	0	0.82	0.82
$b4$	0	0.57	0.57	0	0.57	0.57
$b5$	0	0.42	0.42	0	0.42	0.42
$b6$	0.4	0.55	0.55	-15.8	1.10	1.10
$b7$	0	0.095	0.095	0	0.19	0.19
$b8$	0	0.065	0.065	0	0.13	0.13
$b9$	0	0.035	0.035	0	0.07	0.07
$b10$	-0.156	0.100	0.100	3.63	0.20	0.20
$b11$	0	0.0208	0.0208	0	0.026	0.026
$b12$	0	0.0144	0.0144	0	0.018	0.018
$b13$	0	0.0072	0.0072	0	0.009	0.009
$b14$	-0.1675	0.0115	0.0115	-0.6	0.023	0.023
$a2$	0	0	10	0	0	0
$a3$	0	0.80	0.80	0	0.80	0.80
$a4$	0	0.65	0.65	0	0.65	0.65
$a5$	0	0.43	0.43	0	0.43	0.43
$a6$	0	0.31	0.31	0	0.31	0.31
$a7$	0	0.152	0.095	0	0.19	0.19
$a8$	0	0.088	0.055	0	0.11	0.11
$a9$	0	0.064	0.040	0	0.08	0.08
$a10$	0	0.040	0.032	0	0.04	0.04
$a11$	0	0.026	0.0208	0	0.026	0.026
$a12$	0	0.014	0.014	0	0.014	0.014
$a13$	0	0.010	0.010	0	0.010	0.010
$a14$	0	0.005	0.005	0	0.005	0.005

Table B.3: IT FQ specification `IT_errortable_v5` at 7 TeV. The `ITbody`, `ITcs`, and `ITnc` tables correspond to field errors in the main part of the IT quad and at the two quad ends (connecting and non-connecting sides), respectively.

	ITbody_errortable_v5			ITcs_errortable_v5		ITnc_errortable_v5	
	S	U	R	S	U,R	S	U,R
$b2$	0	0	10	0	0	0	0
$b3$	0	0.82	0.82	0	0	0	0
$b4$	0	0.57	0.57	0	0	0	0
$b5$	0	0.42	0.42	0	0	0	0
$b6$	-0.64	1.10	1.10	8.943	0	-0.025	0
$b7$	0	0.19	0.19	0	0	0	0
$b8$	0	0.13	0.13	0	0	0	0
$b9$	0	0.07	0.07	0	0	0	0
$b10$	-0.11	0.20	0.20	-0.189	0	-0.821	0
$b11$	0	0.026	0.026	0	0	0	0
$b12$	0	0.018	0.018	0	0	0	0
$b13$	0	0.009	0.009	0	0	0	0
$b14$	-0.87	0.023	0.023	-0.545	0	-1.083	0
$a2$	0	0	10	-31.342	0	0	0
$a3$	0	0.65	0.65	0	0	0	0
$a4$	0	0.65	0.65	0	0	0	0
$a5$	0	0.43	0.43	0	0	0	0
$a6$	0	0.31	0.31	2.209	0	0	0
$a7$	0	0.19	0.19	0	0	0	0
$a8$	0	0.11	0.11	0	0	0	0
$a9$	0	0.08	0.08	0	0	0	0
$a10$	0	0.04	0.04	0.065	0	0	0
$a11$	0	0.026	0.026	0	0	0	0
$a12$	0	0.014	0.014	0	0	0	0
$a13$	0	0.010	0.010	0	0	0	0
$a14$	0	0.005	0.005	-0.222	0	0	0

Table B.4: IT FQ specification `IT_errortable_v5` at 450 GeV. The `ITbody`, `ITcs`, and `ITnc` tables correspond to field errors in the main part of the IT quad and at the two quad ends (connecting and non-connecting sides), respectively.

	ITbody_errortable_v5			ITcs_errortable_v5		ITnc_errortable_v5	
	S	U	R	S	U,R	S	U,R
$b2$	0	0	10	0	0	0	0
$b3$	0	0.82	0.82	0	0	0	0
$b4$	0	0.57	0.57	0	0	0	0
$b5$	0	0.42	0.42	0	0	0	0
$b6$	-21.3	1.10	1.10	8.943	0	-0.025	0
$b7$	0	0.19	0.19	0	0	0	0
$b8$	0	0.13	0.13	0	0	0	0
$b9$	0	0.07	0.07	0	0	0	0
$b10$	3.89	0.20	0.20	-0.189	0	-0.821	0
$b11$	0	0.026	0.026	0	0	0	0
$b12$	0	0.018	0.018	0	0	0	0
$b13$	0	0.009	0.009	0	0	0	0
$b14$	0.21	0.023	0.023	-0.545	0	-1.083	0
$a2$	0	0	10	-31.342	0	0	0
$a3$	0	0.65	0.65	0	0	0	0
$a4$	0	0.65	0.65	0	0	0	0
$a5$	0	0.43	0.43	0	0	0	0
$a6$	0	0.31	0.31	2.209	0	0	0
$a7$	0	0.19	0.19	0	0	0	0
$a8$	0	0.11	0.11	0	0	0	0
$a9$	0	0.08	0.08	0	0	0	0
$a10$	0	0.04	0.04	0.065	0	0	0
$a11$	0	0.026	0.026	0	0	0	0
$a12$	0	0.014	0.014	0	0	0	0
$a13$	0	0.010	0.010	0	0	0	0
$a14$	0	0.005	0.005	-0.222	0	0	0